



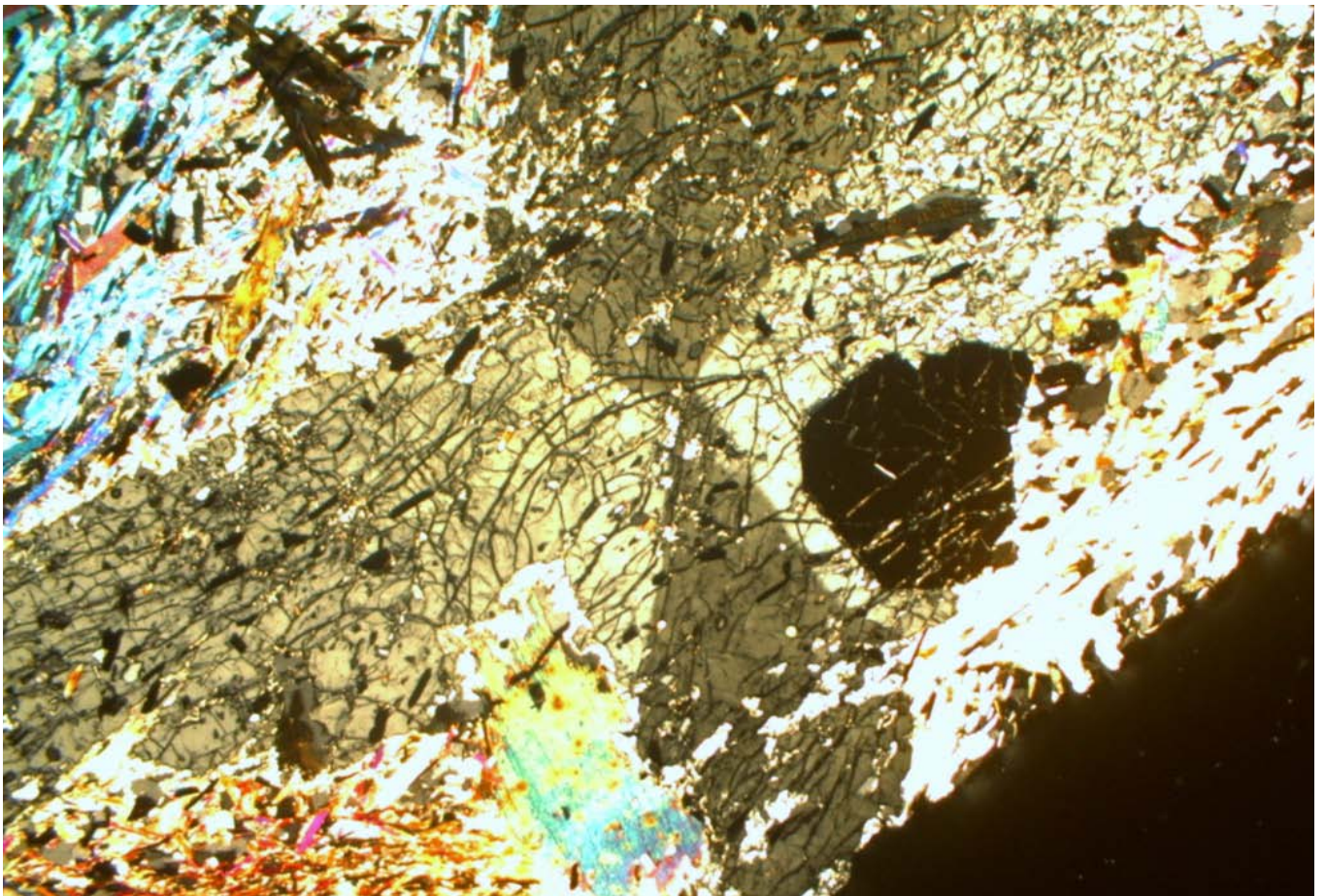
Stockholm
University

Master Thesis

Degree Project in
Geology 30 hp

Differences in staurolite mode due to changes in bulk composition as an effect of mass transfer by fluids during metamorphism

Jonas Nilsson



Stockholm 2014

Department of Geological Sciences
Stockholm University
SE-106 91 Stockholm

Differences in staurolite mode due to changes in bulk composition as an effect of mass transfer by fluids during metamorphism

Jonas Nilsson

Masters Thesis, 30 credits

Department of Geological Sciences, Stockholm University

Abstract

This study is undertaken in the staurolite zone in Glen Esk, Scotland. The area is part of the Dalradian sequence, a sedimentary protolith derived from a shelf in the ancient Iapetus Ocean, that have been metamorphosed through the Grampian tectonic event related to the Caledonian orogeny. Results from petrographic analyses, chemical analyses and mineral phase diagram calculations show that staurolite minerals grew in selvages adjacent to quartz veins. Previous studies show the same relationships between quartz veins and garnet, as well as kyanite growth. The selvages are formed as metamorphic fluids flow through cracks, altering the bulk composition by mass transfer and triggers the nucleation and growth of new minerals. A pseudosection for a staurolite absent sample has been calculated using THERMOCALC. No stability field correlates to visually observed mineralogy. This indicates that a reaction forming staurolite never was triggered since no fluids was present during metamorphism. Peak pressure and temperature is calculated to be ~ 8.5 kbar and ~ 570 °C during metamorphism.

Contents

Introduction	3
Aim	3
Geological Background	4
Previous work in Glen Esk	5
Previous work on fluid flow and selvage formation	5
Previous work on geothermobarometry	6
Methods	7
Field work & Sampling	7
Sample preparation	8
X-ray fluorescence	8
Petrographic analysis	8
Electron microprobe analysis	9
Pressure-Temperature estimates	9
Constructing pseudosections and isopleths	9
Reactions and stoichiometry	10
Results	11
Field work & Sampling	11
X-ray fluorescence	12
Petrographic analysis	13
Pseudosection	20
Pressure- Temperature estimates	24
Discussion	26
Chemical and petrographic analyses	26
Stoichiometry	27
Pressure – Temperature estimates	27
Pseudosections	27
Sources of uncertainty	29
Conclusion	29
Acknowledgements	29
References	30
Appendix	32

Introduction

Aim

This study was undertaken together with Josefin Linde who has conducted similar research parallel to this. The project was supervised by Professor Alasdair Skelton and PhD student Alexander Lewerentz at the Department of Geological Sciences, Stockholm University.

This research focuses on the relationship between metapelites and quartz veins in the Dalradian supergroup of Glen Esk, Angus, Scotland. The aim is to map an outcrop in the staurolite zone, determine chemical composition of the rocks as well as peak pressure and temperature at the metamorphic event. Specifically, this thesis aims to confirm or deny any spatial correlation between quartz veins and changes in rock composition, referred to as 'selvages'. If staurolite crystals are larger and/or in higher mode within selvages, the aim is also to determine whether it is due to mass transfer of elements between quartz veins and wall rock, and if this correlates to fluid flow during metamorphism. To elucidate any eventual relationships between the rock types in the outcrop; quartz veins, wall rock and selvages, a P-T pseudosection of stable mineral phases is presented for a staurolite-absent sample. This is compared with a P-T pseudosection of staurolite-present sample constructed by Josefin Linde (2013).

Figure 1 is part of a map taken from George Barrow (1912) and shows the staurolite zone in relation to the other metamorphic zones in Glen Esk.

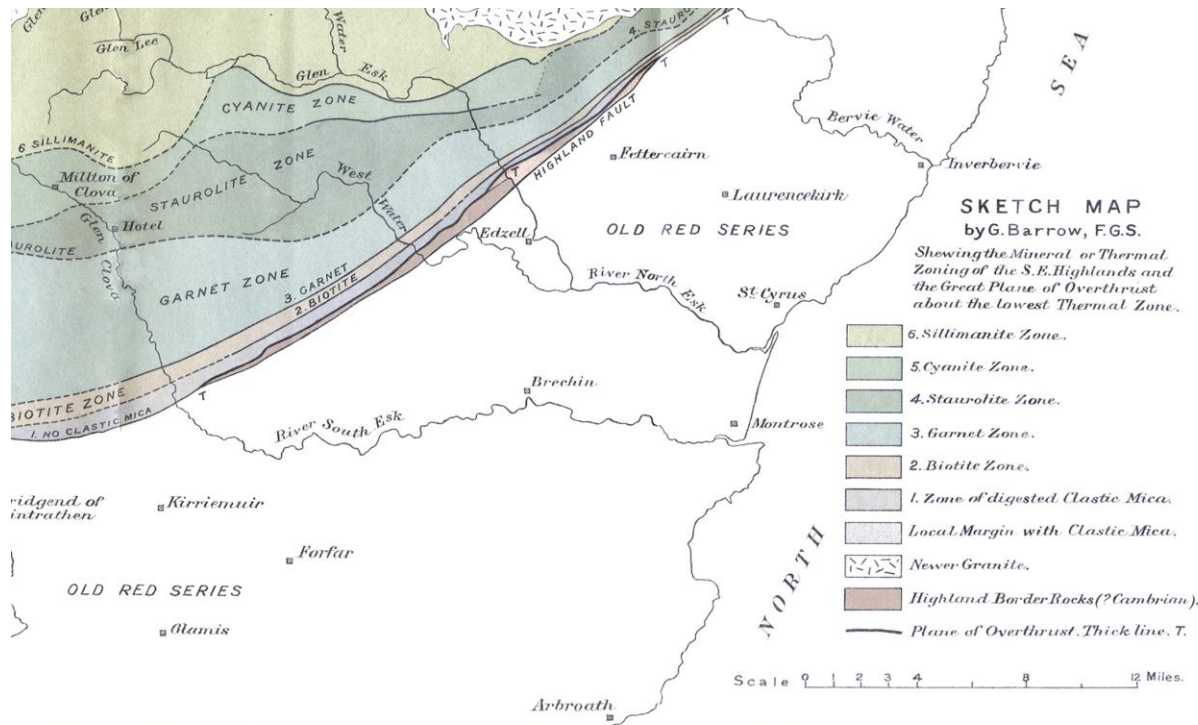


Figure 1. Part of a map, drawn by George Barrow, showing the metamorphic zones north of the Highland border in Scotland.

Geological Background

Glen Esk in Scotland is known for the concept of Barrovian metamorphism and is one of the places George Barrow visited while developing the hypothesis of metamorphic zones. These zones represent pressure and temperature conditions during metamorphism required for certain minerals to grow. The index minerals of the Barrovian metamorphic zones were clastic and digested clastic micas, biotite, garnet, staurolite, kyanite and sillimanite from low grade to high grade metamorphism (Barrow, 1912). The zones of 'clastic micas' and 'digested clastic micas' were later reworked to one 'chlorite' zone by Tilley (1925).

The outcrops in Glen Esk are mainly metapelites that are part of the Dalradian supergroup which comprises several sedimentary protoliths. Figure 2 shows the Dalradian in relation to older metasediment sequences in the Scottish Highlands. These protoliths have been metamorphosed through the Grampian tectonic event related to the Caledonian orogeny where Laurentia, Midland Valley arc and Baltica collided, finally closing the Iapetus ocean some 500 million years ago (Tanner, et al. 2013). Much of the metasediments that make up the Dalradian were turbidites, sandstones, clay/mudstones and greywackes deposited on and near a passive continental margin of Laurentia (Tanner, et al. 2013; Stephenson, et al. 2013; Fettes, et al. 2011). Figure 3 is a geological map taken from Tanner et al. (2013) and shows the different metasedimentary rocks within the Dalradian supergroup. Point 10 in the map is Glen Esk. The map also features igneous intrusions related to the Caledonian orogeny (Tanner, et al. 2013; Vorhies and Ague, 2011).

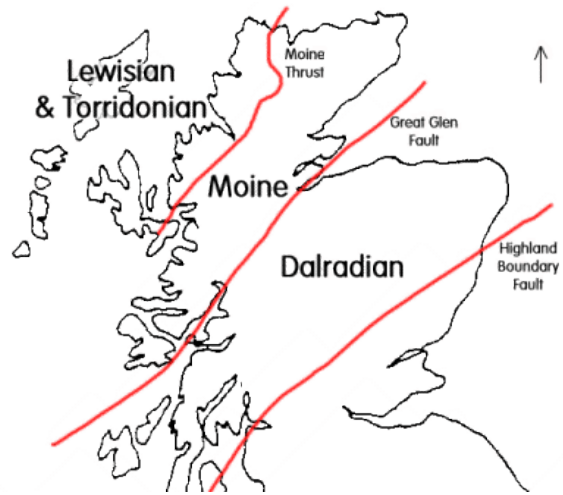


Figure 2. Map of northern Scotland with different metasedimentary sequences. From www.geologyrocks.co.uk (2013).

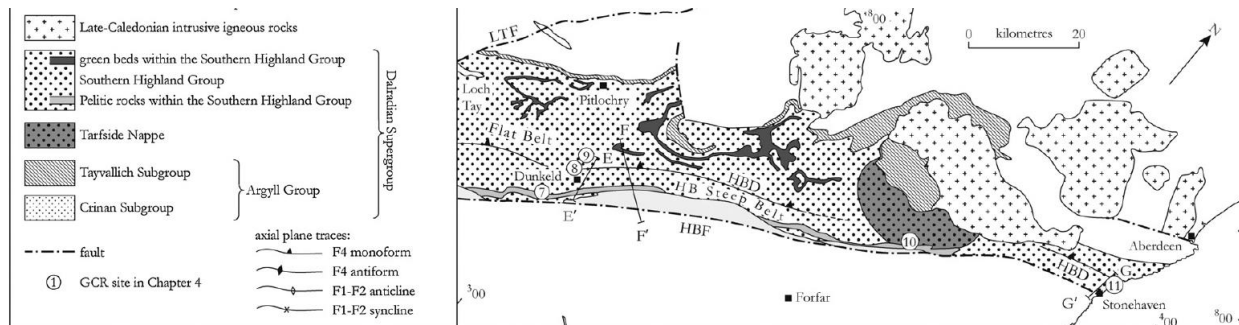


Figure 3. Geological map by Tanner, et al. (2013). Point 10 shows Glen Esk within the Dalradian supergroup.

Previous work in Glen Esk

Barrow (1912) describes in his excursion guide to Glen Esk how the rocks become more crystalline towards north-west and that the appearance of index minerals depends on the 'isothermals', parallel segments in the sequence where index minerals first appear one at a time.

The Grampian tectonic event was relatively short in time compared to most other known orogenies. Collision and prograde metamorphism by crustal thickening is believed to have happened 475 – 467 Ma according to models from Dewey (1997). Peak temperature and pressure from lower kyanite to upper sillimanite zone in nearby Glen Clova have been calculated, using a number of solid solution geothermometers and geobarometers, by Baker (1985) to be ~540 – 800 °C and ~5.5 – 10 kbar in Glen Esk. Vorhies and Ague (2011) concludes the peak metamorphic temperatures to range from ~500 to ~650 °C and pressures ranging from ~5 to ~8 kbar from garnet to sillimanite zone in both Glen Clova and Glen Esk.

Vorhies and Ague (2011) also describe the Barrovian zones in greater detail and present further evidence for a series of intrusions that by thermal pulses increased the temperature during metamorphism. The intrusions are featured in the geological map by Tanner, et al (2013) in figure 3. These pulses distributed heat through conduction as well as by motion of magma and fluids through the rock (advective heat). Garnet zoning, as a result of different growth conditions, is considered to be related to these thermal pulses. By this, together with previous zircon and garnet dating, Vorhies and Ague (2011) conclude that peak temperature happened through a relatively short time interval, c 10 M years, with beginning at about 470 Ma when the Grampian event had stopped and thermal relaxation provided conditions for several intrusions. These intrusions are considered a significant factor for advective heat transfer in the metamorphosed Barrovian zones that can be seen today in the Scottish Highlands (Lyubetskaya & Ague, 2009).

Previous work on fluid flow and selvage formation

Recent work suggests that mass transfer of major elements like *Fe*, *Mg*, *Al* and *Si* is due to the infiltration of fluids related to metamorphism, and that the loss of silica (SiO_2) from the host rock to an adjacent quartz vein may result in a chemical composition that favors the growth of index minerals (Ague, 2011; Nabelek, 1997). In this study, the silica loss as well as the bulk composition of protoliths, has been considered a possible key factor for the chemical composition of rocks seen in Glen Esk. Figure 4 is a simple schematic picture of the selvages, rich in index minerals, adjacent to the quartz vein.

In a study, Ague (2011) presents evidence for mass transfer related to fluid flow in a research conducted in Wepawaug Schist, Connecticut, USA, where the area had gone through Barrovian metamorphism. The conclusion is that the analyzed veins consist of quartz derived both from regionally and locally transferred silica (SiO_2) of ~40% and ~60%, respectively. The loss of silica from the host rock to the veins results in an area adjacent to the vein referred to as a selvage. This selvage has a relative enrichment in

iron (*Fe*) and aluminium (*Al*) which is due to the mere relation to silica loss, but also due to the small addition from the nearby fluids.

Skelton (1997) conducted a study on a schist in north Norway and suggested that garnet nucleation and growth depends on the fluid flow through the rock during metamorphism. The study shows that garnet nucleation increases within a selvage next to where fluids are channeled, while the garnet growth increases within a selvage next to where fluids are pervasive.

'Pervasive flow' in this case, means that the fluids move along smaller conduits in slow pace in contrast to 'channeled flow' when fluids flow through larger conduits in a faster pace.

A summary of studies by Ferry (1994) explains the importance of fluid flow during metamorphism and that chemical reactions in rocks often are driven and/or triggered by the infiltration of fluids such as H_2O and CO_2 and that solubility of SiO_2 increases with increasing pressure and temperature.

Garnet size and abundance is believed to be controlled by the loss of silica in metapelites. This is observed in three areas in the garnet zone in Glen Esk, Scotland and results are presented by Lewerentz et al. (2014) in an ongoing study to determine the relationship between index mineral growth and quartz veins.

Minerals that formed tens of km down in the earth's crust can be found at the surface today, often in euhedral shape and according to visual examination, often at stable conditions. This is because the minerals have not recrystallized during exhumation. Walther (2013) explains this process by the lack of fluids. Metamorphic fluids that have been released by dehydration during prograde metamorphism escapes through conduits and cools off or become incorporated in new hydrated mineral crystals like amphiboles, muscovite and chlorite.

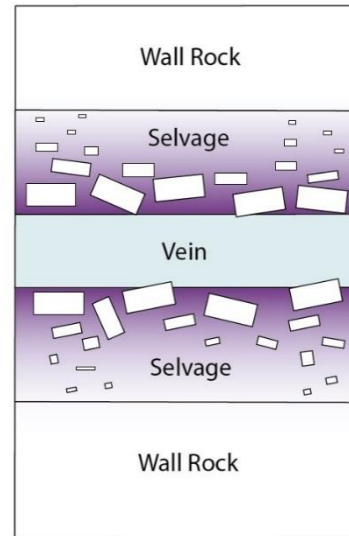


Figure 4. Schematic sketch of selvages (gradient fields) containing mineral crystals (white squares) in decreasing sizes away from the quartz vein.

Previous work on geothermobarometry

Experimental studies on element distribution among minerals at different pressure and temperature conditions have provided tools for constructing pressure and temperature (P-T) estimates and mineral phase diagrams. Mineral end members favor certain elements within their structure dependent on pressure and/or temperature (Kohn & Spear, 2000; Ferry & Spear, 1978; Winter, 2011). A data set based on empirically derived data, compiled by Holland and Powell (Powell, et al. 1998; Holland & Powell, 1998), is often used for geothermobarometric calculations.

Methods

Field work & Sampling



Figure 5. Research area in relation to the cities Edzell, Stonehaven and Aberdeen in Scotland. Adapted from a map taken from www.westscotland.com (2013).

Accommodations during the field work was at the town of Edzell. The research area in the staurolite zone was reached by a car drive of about 15 minutes to Auchmull followed by a walk of about 15 minutes up to 'Craig of Weston' ($56^{\circ} 51' 55''$ N, $2^{\circ} 41' 37''$ W). Figure 5 shows the research area in spatial relationship to Aberdeen, Stonehaven and Edzell.

The area was mapped and a number of profiles were drawn on the outcrops. This was made as a spatial reference for point counting minerals as well as determining the exact location of samples. Profiles consisted of two-dimensional series of $3 \times 3 \text{ cm}^2$ squares. The profiles were drawn perpendicular to the apparent bedding/lamination and foliation with the assumption that the rock chemistry is consistent throughout the layers, at least within the considered outcrop. Samples were taken with hammer and chisel. Due to the lack of precision when sampling this way, some samples are not taken within the profile squares directly, but still represents the layers in the rock. See figure 6.



Figure 6. Picture shows profiles with $3 \times 3 \text{ cm}^2$ squares on outcrop in the field.

Sample preparation

Samples were prepared before analyses by sawing and polishing before making thin sections as well as crushing and milling before performing chemical analyses. This was done at the Department of geological sciences, Stockholm University under supervision of Dan Zetterberg.

'Loss on ignition' (LOI) was measured for determining the amount of adsorbed water and other volatile substances in the samples. Samples were weighed after 10 hours at 105°C to determine loss of adsorbed water. The samples were weighed again after 10 hours at 1000°C to determine loss of structural water, for example in hydrous minerals. The weights recorded could thereafter be compared to the initial weight. A weight gain at this point could indicate high amounts of iron that oxidizes and incorporate more oxygen. The extraction of the OH component in hydrous minerals requires at least 800°C (Winter, 2010), the intervals are hence considered more than enough for a reliable result.

To acquire reliable results from XRF analysis, the samples that had gone through LOI were made into glass disks. This is done to ensure homogeneity in sample chemistry (Alvarez, 1990).

While sampling and preparing, abbreviations for the samples were set to be *Research area, Outcrop, Profile – Square*, as for example; **B21-5-6** (area **B**, outcrop **2**, profile **1**, square **5 to 6**). This is the working standard for this report. For technical details regarding sample preparations, see appendix B and C.

X-ray fluorescence

X-ray fluorescence (XRF) analysis was done for determining the weight percent of elements in their oxidized form which is considered to be the normal amount of oxygen bounded to each ion in typical silicate minerals (Winter, 2010). Although the XRF device counts pure element concentrations (Pettersson, et al. 1997) the raw data is presented as oxides, eg: SiO_2 . Ferric iron (Fe_2O_3) is recalculated as ferrous iron (FeO). The XRF-analysis was performed under supervision of Runa Jacobsson. See Appendix D for technical details.

Petrographic analysis

Using a microscope with plane and cross polarized light, minerals as well as reaction textures and strain textures were identified. This method is good as it gives clues to mineral growth as well as the ability to determine whether minerals are in equilibrium in relation to each other, which is very important for further geothermobarometric calculations. See appendix E for microscope details.

Point counting is a way of determining modal percentage of minerals; the total area different kinds of minerals occupy within the thin sections. This was done with microscope and point counting machines

as a compliment to point counting in the field. All thin sections were counted at 1000 points each and five samples/thin sections were selected for point counting in 10 rows parallel to foliation/lamination for determining modal differences at higher resolution. See appendix I for mineral abbreviations and chemical formulas (Nesse, 2009).

Electron microprobe analysis

Electron microprobe (EMP) analysis was done at the Department of Earth Sciences, Uppsala, under supervision of Jaroslaw Majka. Two types of analyses were performed; wavelength dispersive spectrometry (WDS) and energy dispersive spectrometry (EDS). WDS acquired high precision of chemical composition in a small area (1-3 μm) of one crystal at a time, which was later used for calculations of stable mineral phases. EDS was used to confirm mineralogy seen in thin sections and it also gave clues to if chemical reactions had occurred in and near crystal rims. See appendix F for output-data and technical information.

Pressure-Temperature estimates

Pressure and temperature (P-T) estimates gives indications to the pressure-temperature conditions during peak metamorphism. EMP data gives the chemical composition of each examined mineral crystal and the composition is used by a software called AX2 to calculate the 'activity' for the mineral phases. The activity is a value assigned to a component in a system and represents the availability of that exact component to participate in a certain reaction. The activity is based on the chemical potential, the differences in chemical composition between components (Winter, 2011). The activity is a coefficient used for further calculations in THERMOCALC softwares and ranges from 0 to 1, low to high activity. Once the activity for the mineral phases in the sample had been calculated by AX2, other calculations were done in THERMOCALC 3.33. The output were P-T conditions at peak metamorphism as well as the respective standard deviations. The softwares are developed, and the thermobarometric data set is compiled by Holland and Powell (Powell, et al. 1998; Holland, et al. 1998). The thermobarometric data used in this study is compiled from experimental data from White, et al. (2007), Holland & Powell (1998) and Holland, et al. (1998b).

Constructing pseudosections and isopleths

Calculations for the pseudosections were made in THERMOCALC 3.37 with a prewritten script file for a KFMASH (K_2O , FeO , MgO , Al_2O_3 , SiO_2 , and H_2O) bulk composition (Holland & Powell, 1998). The composition were taken from XRF data, corrected for Al_2O_3 and SiO_2 tied up in plagioclase as well as FeO tied up in iron oxides, and normalized to mole percent. Since rocks are sampled from an area which is part of a larger sequence of one rather consistent bulk composition, assumption is made that the metapelite could develop all mineral phases which is seen in the general area. Therefore, an invariant

point where both staurolite and bordering kyanite, as well as biotite, muscovite, garnet and chlorite are stable were calculated as a starting point for the pseudosection. From invariant points, lines where phases go out at pressure and temperature intervals, as well as potential reactions, were then calculated. See figure 7. This was done according to Schreinemaker's rules (Winter, 2010) and with the assumption that all mineral phases in the samples are in equilibrium in relation to each other.

The partitioning of elements in mineral crystals are dependent on temperature and/or pressure (Ferry & Spear, 1978; Kozoi & Newton, 1988; Hoisch, 1990). For example, the partitioning of Fe/Mg in biotite and garnet is temperature dependent and often very reliable (Ferry & Spear, 1978) for making calculations of geothermometry. This fact allows the construction of isopleths on stability fields in a pseudosection. Isopleths are lines within a stability phase field representing constant chemical compositions. Isopleths for $Fe/(Fe+Mg)$ -ratios in garnet and $Al/(Al+Mg+Fe)$ -ratios in muscovite for the geometric M2 position were added on stability fields where both mineral phases exist and by calculating the actual partitioning using EMP-data, an intersection was derived, representing a narrow P-T window.

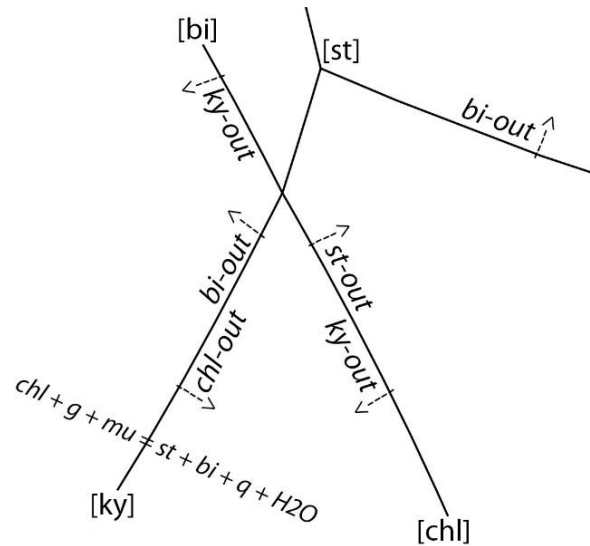


Figure 7. The beginning of a pseudosection. Using Schreinemaker's rules and reactions acquired from THERMOCALC, reaction-lines, out-lines and stability fields begin to take shape.

Reactions and stoichiometry

Using the reactions at different P-T conditions acquired from THERMOCALC 3.37, stoichiometric calculations were made to find out the ratios of reactants and products in the rock at peak metamorphic conditions. Using average crystal densities for each mineral (www.webmineral.com, 2013), the calculated area any specific mineral should accommodate was then compared to point counting results. This was done to determine whether any one mineral should accommodate larger area than what was seen in the thin section. If, for example quartz, should have been produced in larger amounts than was seen, the conclusion would be that quartz had been removed from the rock.

Reactions were closely examined as they were calculated by THERMOCALC. Questions considered were; Are the mineral phases in reactions visually confirmed to exist within the samples? Are there any reaction textures in the thin sections indicating that any of these reactions have occurred, whether it being prograde or retrograde? Reactions generated by THERMOCALC were considered plausible but not necessary.

Results

Field work & Sampling

Area of focus is locality B where five outcrops are visible. By visual examination, the outcrops display big differences in appearance. Outcrops 3 and 4 are mainly pelitic, extremely weathered and contain big crystals of staurolite and garnet. By comparing the pelitic layers with psammitic laminations, both in covered and uncovered positions, weathering rates are estimated to be up to 5 mm/year. Outcrops 1 and 5 are more psammitic and less weathered and display medium sized garnets and no observed staurolite. Outcrop 2 display a variety of pelitic and psammitic beds with sporadically distributed veins in different sizes and shapes.

The locality is measured and schematically sketched to highlight the spatial relationships between outcrops. The general strike of lamination and foliation is 40° azimuth and dip is of approximately 90° with the exception for outcrop 1 which has a dip of about 65° . The sketch below, Figure 8, illustrates the research area and features profiles where samples were collected.

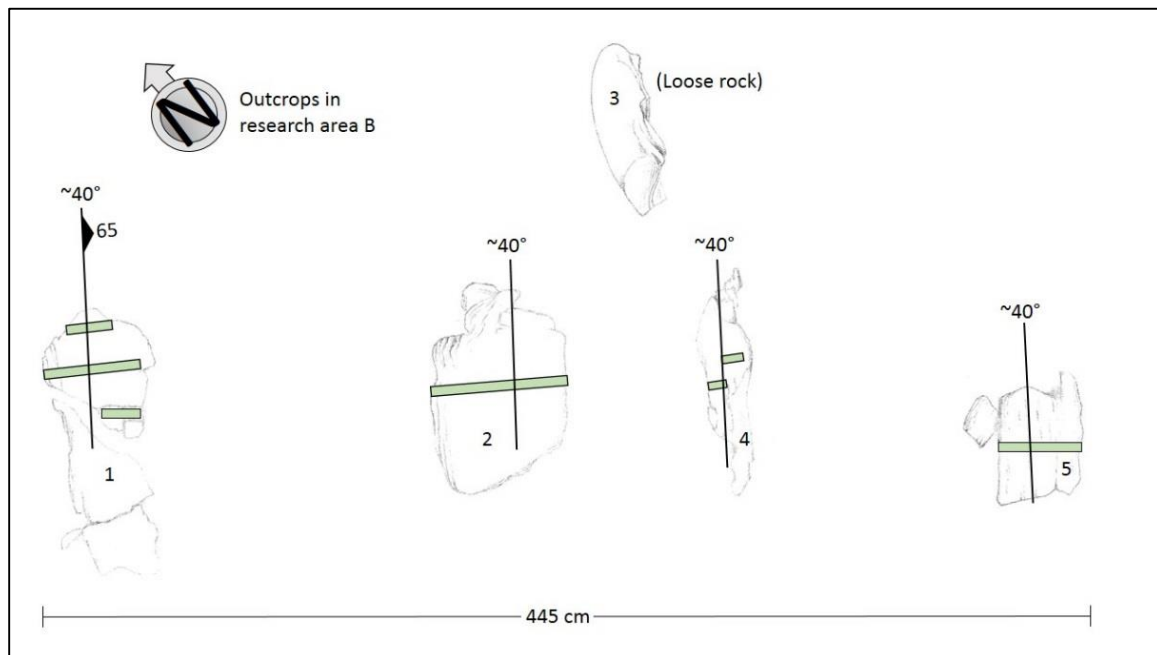


Figure 8. Schematic sketch of outcrops in locality B including strike and dip of bedding/lamination and profiles (green elongated fields) for sampling.

X-ray fluorescence

XRF-results in figure 9 show differences in oxide distribution throughout the profiles. Focus has been on outcrop B1 since it consists of areas both with and without staurolite. One visible trend is in profile 1 (combined with profile 2) where inverse amounts of SiO_2 compared to Al_2O_3 , FeO , K_2O and TiO can be seen, while Na_2O roughly follow the SiO_2 line. Other oxides show no trends. SiO_2 amounts are corrected for the quartz vein density in samples B11-8 and B11-10 while veins in B12-4-5 and B12-6 were impossible to remove before XRF-analysis.

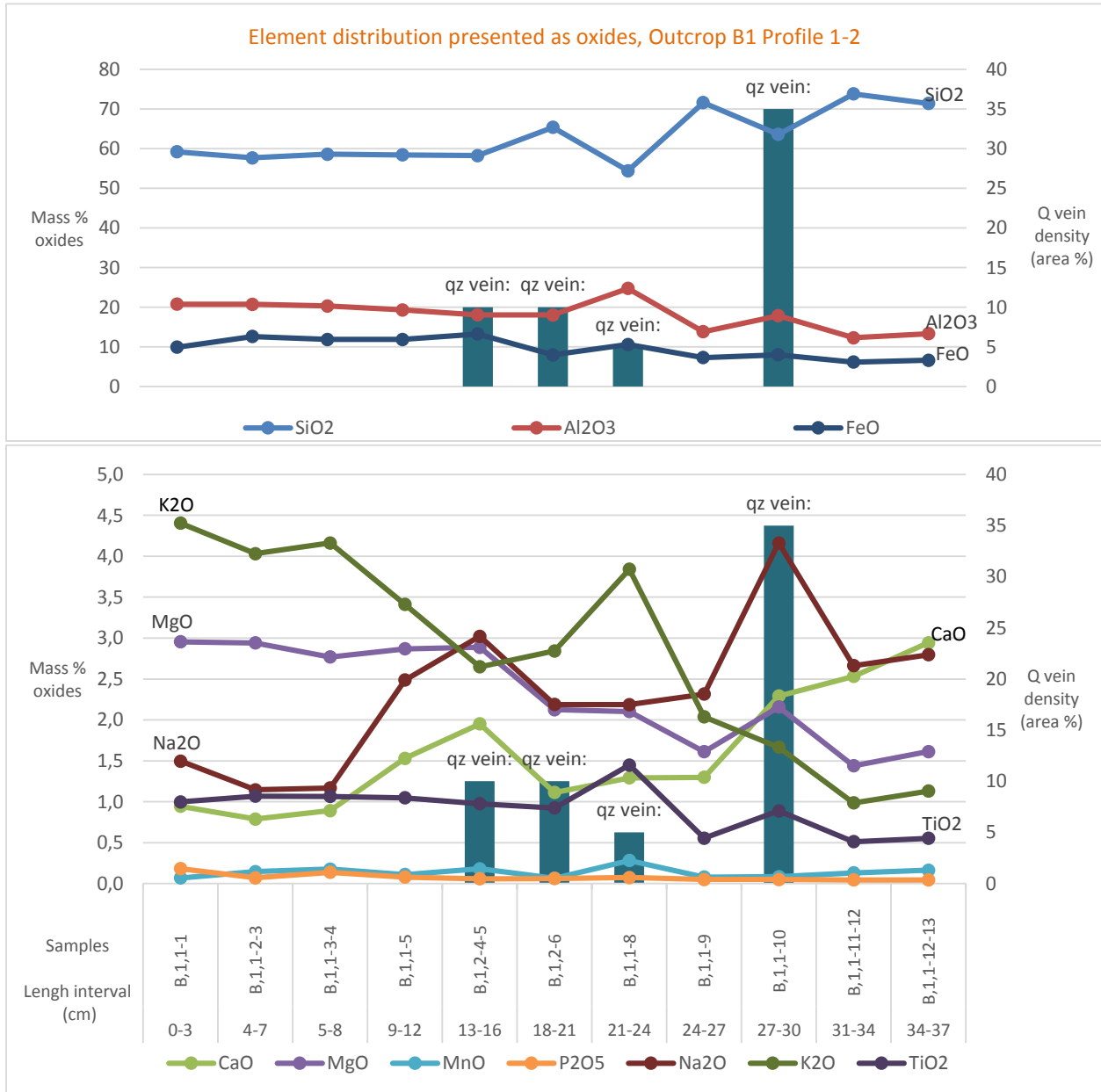


Figure 9. Distribution of oxides throughout profile 1 (and 2) in outcrop B1. Lines represent % oxides and bars are estimated vein density from field observations. The figure is divided into 2 graphs to visualize both large and small differences on the y axis.

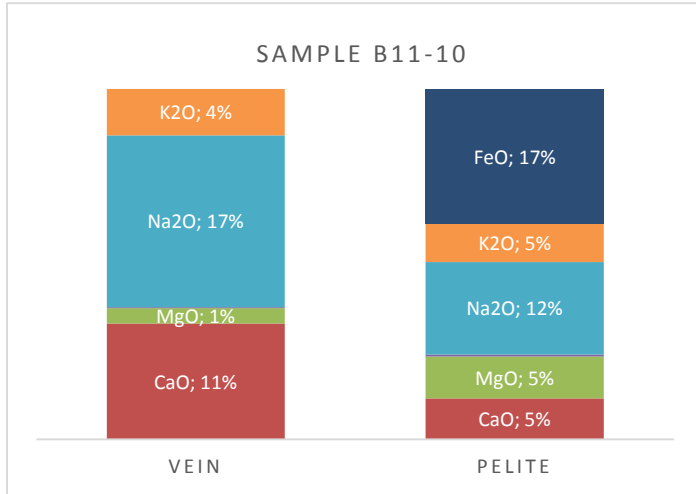


Figure 10. Graph shows the difference in oxide distribution between vein and the adjacent pelitic part.

The vein in sample B11-10 is compared to the pelitic part next to it. Oxides are normalized to all measured oxides except SiO_2 while MnO , P_2O_5 as well as TiO_2 are left out since they are next to zero for both columns. FeO is not present in the vein and K_2O and MgO are more abundant in the pelite as they constitute most of the micas and index minerals. Na_2O and CaO are more abundant in the vein, probably tied up in plagioclase which make up a lot of the vein. This is shown in figure 10.

For LOI-data, see appendix A and for XRF-data, see Appendix D.

Petrographic analysis

Petrographic analysis has been performed on samples both with and without staurolite. The analysis shows a number of minerals both in, what seems like, equilibrium and disequilibrium. Most of the index minerals (chlorite, garnet, biotite and staurolite) are euhedral to subhedral but a few minerals show reaction textures between each other. Evidence of reaction does not only show as texture in thin sections but also from EMP-data. For example, chlorite and muscovite appear in the shape of staurolite in figure 11 and garnet is in reaction with staurolite in figure 12.

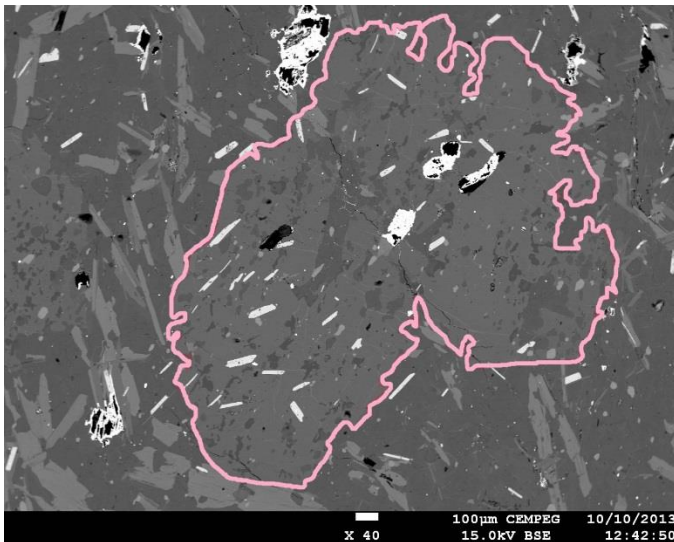


Figure 11. Picture shows staurolite crystal with chlorite chemistry. Picture from back scatter electron detector (SEM-BSE).



Figure 12. Picture showing staurolite (blue outline) reacting with garnet (green outline). Picture is viewed through plane polarized light.

Figure 13 shows staurolite, garnet and biotite which all have been crystallized syntectonic. This can be seen as garnet was crystallized first and while stress was applied, garnet broke up and recrystallized at the same time as staurolite and biotite began to grow. Garnet could also have been replacing biotite or staurolite. No reaction texture can be seen. Figure 14 shows a staurolite crystal with ideal cross-twinning with some garnet inclusions. Figure 14 shows a staurolite crystal with ideal cross-twinning with some garnet inclusions.

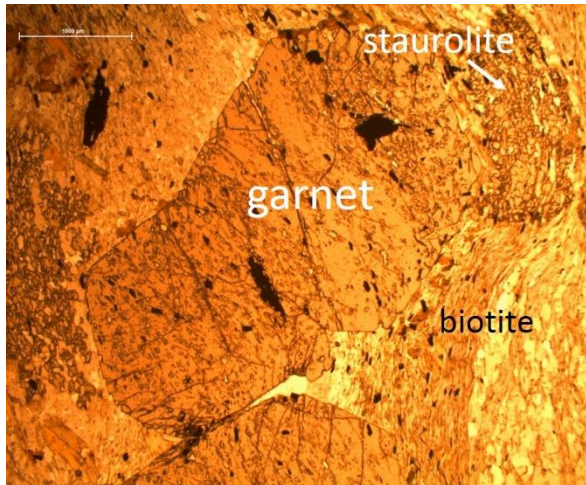


Figure 13. Staurolite, garnet and biotite growth indicating syntectonic crystallization. Picture is viewed through plane polarized light.

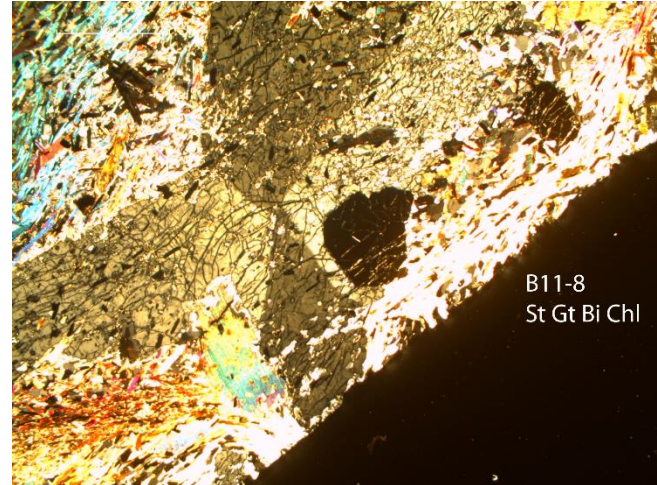


Figure 14. Euhedral staurolite crystal (twinning texture) with garnet inclusions (dark patch) surrounded by biotite and chlorite. Picture is viewed through crossed polarized light.

By looking only at garnets, most of the crystals are euhedral and EMP-data show trends of increasing Mn toward the rims. EMP-data shows that the almandine/pyrope ratio is overall higher toward the rims. See appendix F for EMP-data of garnets.

As well as identifying minerals and reaction texture, point counting was performed on all samples. Focus has been on outcrop B1 and the two profiles crosscutting it since this outcrop features most mineralogical differences. Figure 15 shows spatial relationship between samples/thin sections and profile elongation. Staurolite is present in samples B11-1 to B11-10 and absent in samples B11-11-12 to B11-12-13.

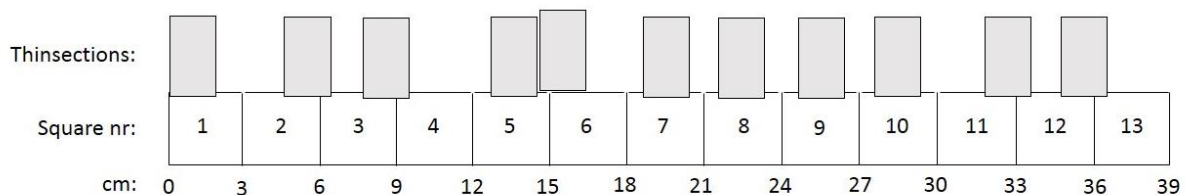


Figure 15. Picture shows the spatial relationship between thin sections and the profile B11.

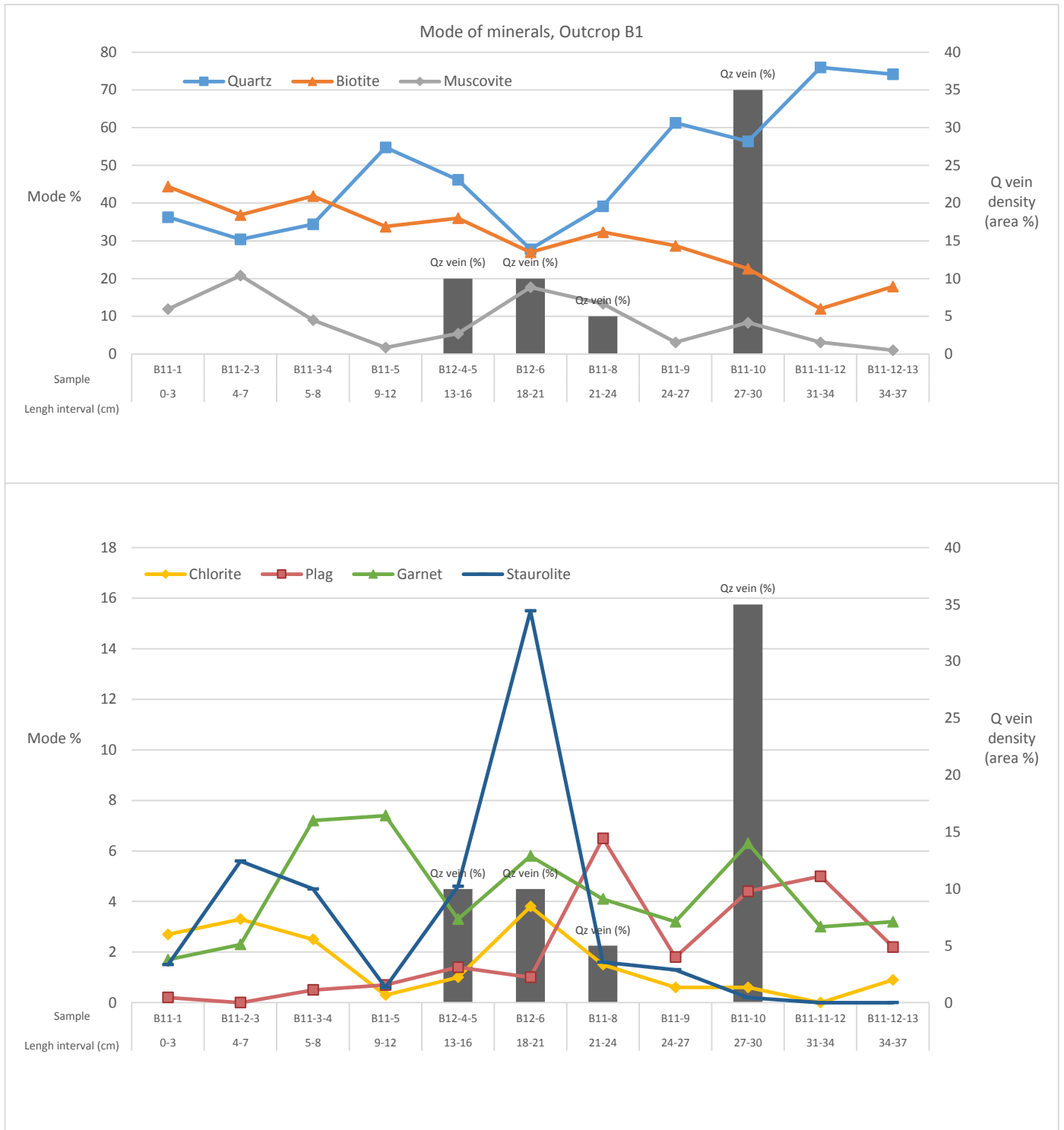


Figure 16. The lines represent mineral modes in profile 1 (and 2) in outcrop B1. The bars represent vein density. The figure is divided into 2 graphs to visualize both large and small differences on the y axis.

Results in figure 16 show differences in mineral mode throughout the entire profile B11 with no big trends in correlation to vein density, but by zooming in to a few thin sections in the middle of the profile (figure 17), trends can be seen. Between B11-4-5 and B11-10, chlorite seems to be the inverse of garnet and the biggest differences between the two appears next to the veins where chlorite is minimal. These values are normalized to all mineral modes except quartz and oxides to see correlations regardless of whether the rock is psammitic or pelitic. Staurolite mode is not as clear when searching for a pattern, but accommodate largest areas next to the veins, show inverse of chlorite mode in some areas and are in low mode % where the rock contains high amounts of SiO_2 .

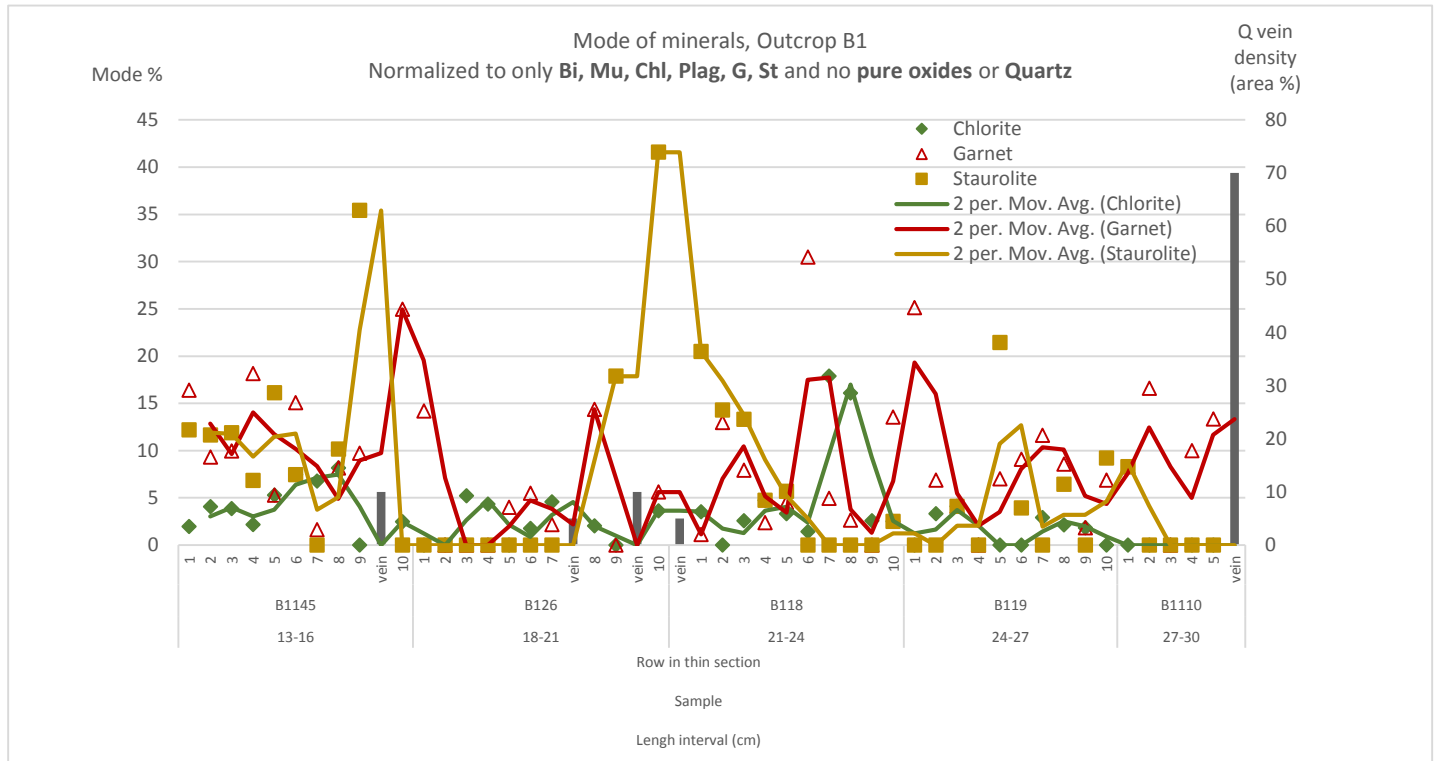


Figure 17. Data points and trend lines for chlorite, garnet and staurolite from high resolution point counting in B11 and B12.

Most of the samples contain staurolite, garnet, biotite, chlorite, muscovite and quartz and figure 12 shows a reaction between garnet and staurolite. For that reason, assumption is made that several reactions involving these minerals have occurred during metamorphism. By looking at the differences between the reactants and products of a staurolite-in reaction, $chl + g + mu = st + bi + q + H_2O$ (unbalanced), areas between the veins display very big differences. This is visualized in the graph (figure 18) by a trend line.

For comparison, a line representing a garnet-in reaction is added to the graph (figure 19). The garnet-in reaction, $chl + mu + q = g + bi$ (unbalanced), is not acquired from THERMOCALC but considered plausible to have happened at some point because of the visible mineralogy in all of the samples. Both reactions are represented as trend lines and the graph features vein densities. The lines are not perfectly similar as inverse of each other but show maximum and minimal ratios in the same general areas in the profile, which indicates areas of high and low reaction rates, no matter the reaction.

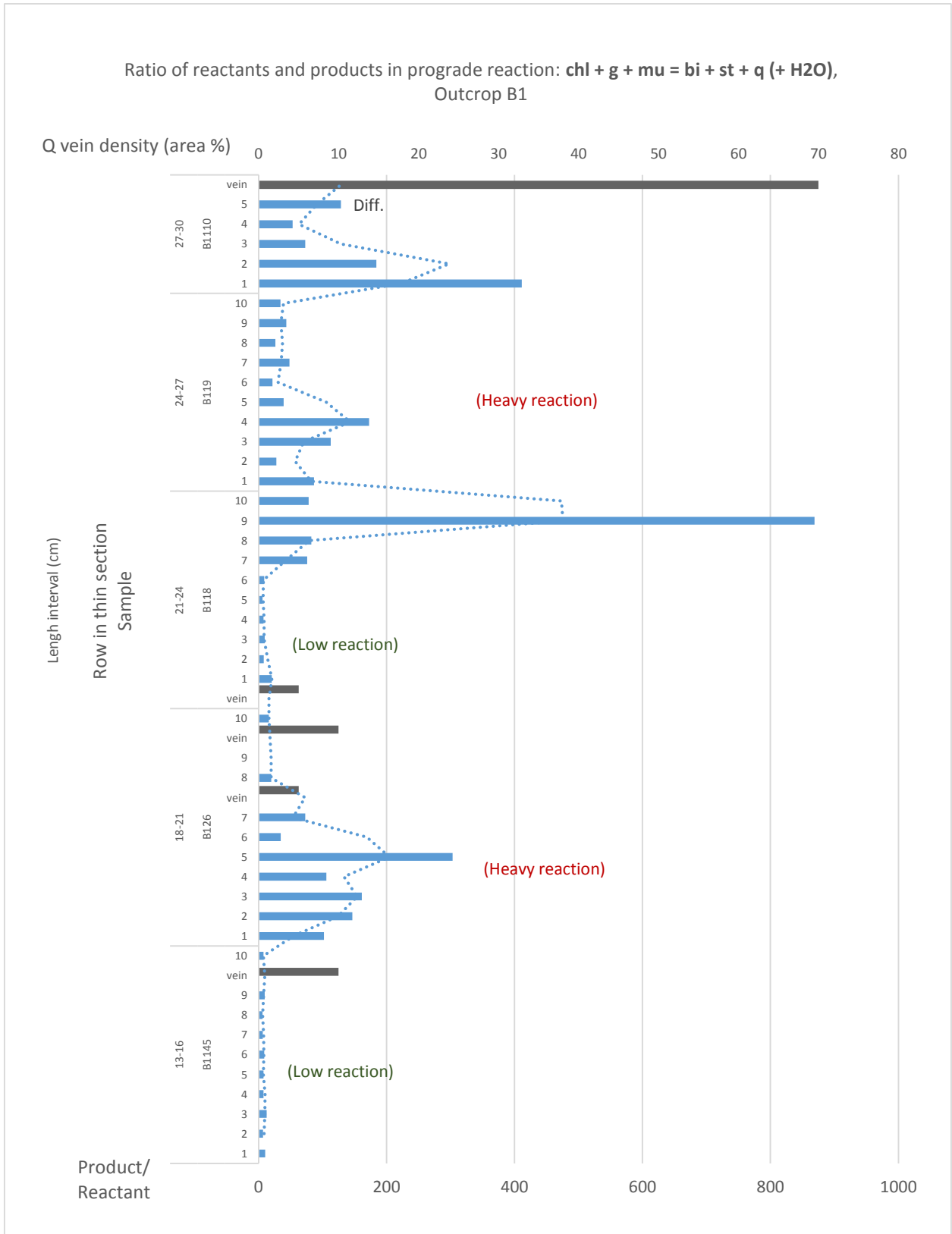


Figure 18. Blue bars with trend line indicates ratio of product/reactant for a staurolite-in reaction (lower x axis) while grey bars represent vein density (top x axis) throughout the profile. Sample names and length interval is displayed next to the y axis.

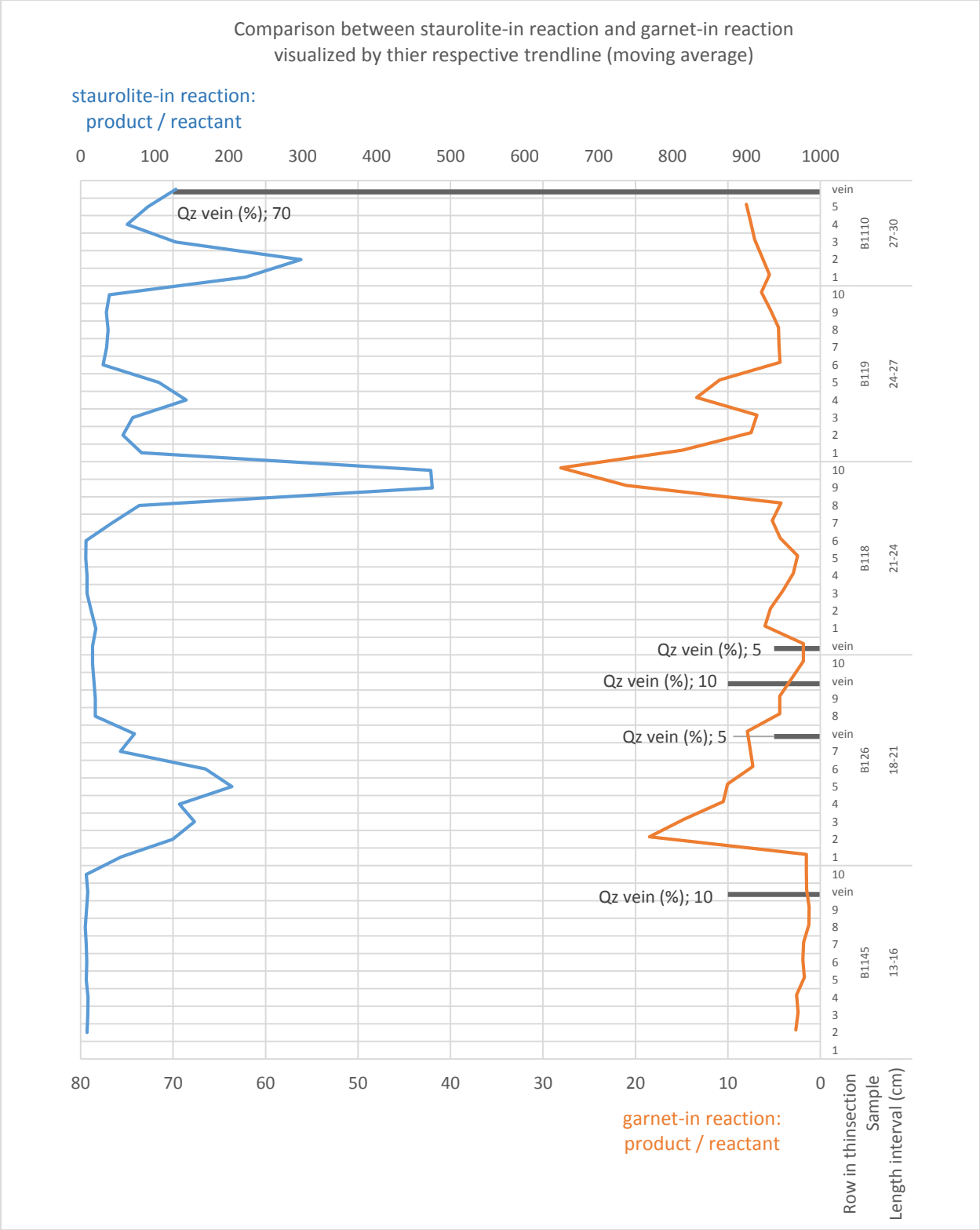
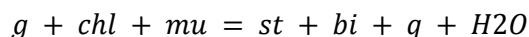


Figure 19. Blue trend line to the left represents product/reactant ratio for a staurolite –in reaction (top x axis) while orange trend line represents product/reactant ratio for a garnet-in reaction (lower x axis). Sample names and length interval is displayed next to the y axis.

For a staurolite-in prograde reaction there is a change in ratio between some minerals as elements are redistributed among the products. By calculating an average ratio of mineral crystal units in the reaction that occur through a certain P/T interval, it is possible to compare the ratios with mineral mode in the thin section. By this method it is possible to calculate any imbalance in mineral mode, to determine if any mineral is lacking or overrepresented in the sample. Below, in table 1, is the average ratios of minerals in the reaction;



which is calculated by THERMOCALC 3.37 from any given bulk composition.

For every chlorite, it takes certain amounts of garnet and muscovite, and for every staurolite it takes certain amounts of biotite, quartz and water to balance the reaction. Since water is considered to have been removed during a very short time, it is also removed from the average ratios. Mineral abbreviations can be found in appendix I.

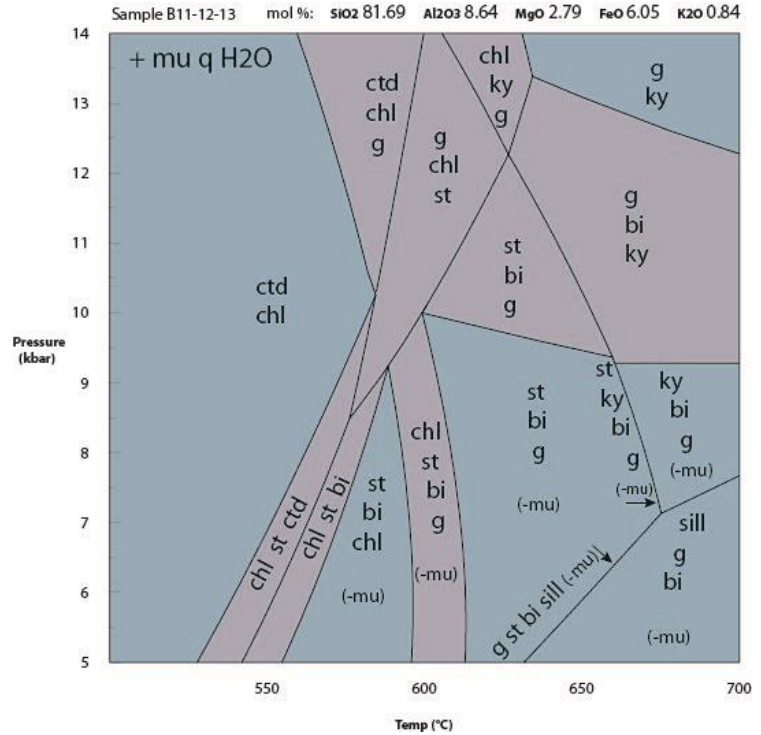
Table 1.	Reactants			Products		
<i>Mineral:</i>	<i>g</i>	<i>chl</i>	<i>mu</i>	<i>st</i>	<i>bi</i>	<i>q</i>
<i>Ratios:</i>	1.2	1	2.7	1	6.2	10.4

A number of kyanite-in reactions were generated as well, but not considered plausible since no kyanite were found in any of the samples. When looking at mineral modes in the profile B11 and B12, it can be seen that in some samples the staurolite mode is very high. For example, in sample B12-6, staurolite mode is 15.5 %. This means that the same sample should contain roughly 51 mode % biotite and 12 mode % quartz. Mineral mode from sample B11-6 shows that this is not the case. Biotite mode is ~ 27 % and quartz mode is ~ 28 % even with vein density disregarded. Several reactions were considered but not pursued further in this test since visually observed mineralogy did not render them very plausible. For complete petrographic data, see appendix E.

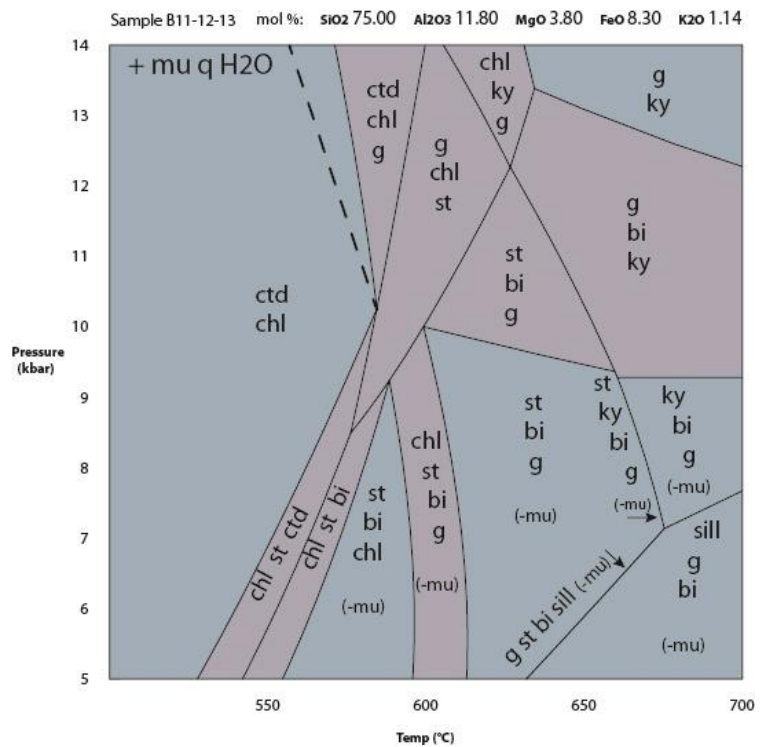
Pseudosection

Pseudosection 1 shows fields of mineral phases where they are stable together as a function of pressure and temperature for a given bulk composition. This pseudosection is constructed from staurolite-absent sample B11-12-13 and it is calculated from the bulk composition seen in the top of the pseudosection. Muscovite, quartz and water are visible as in excess. Muscovite is considered to be in all phase fields except for the seven lower right fields. Quartz is also considered to exist within all phase fields. Water is always present in the calculations and considered to be in excess at all times. It is interesting to note that pseudosection 1 contains two fields that appears to be lines which contains biotite, garnet, sillimanite and staurolite as well as staurolite, kyanite, biotite and garnet.

To answer the question if the growth of staurolite is related to fluid flow, hence quartz vein formation, it is interesting to see if the changes of SiO_2 effects the staurolite growth. To see the potential effect of changes in SiO_2 -amount, a second pseudosection (2) is calculated with a 'made up' bulk composition that contains the same proportions of Al_2O_3 , MgO , FeO and K_2O but with lower SiO_2 content. Bulk composition can be seen in the diagram. Dashed line in pseudosection 2 indicates the only visible difference between the two pseudosections; the garnet-out line.

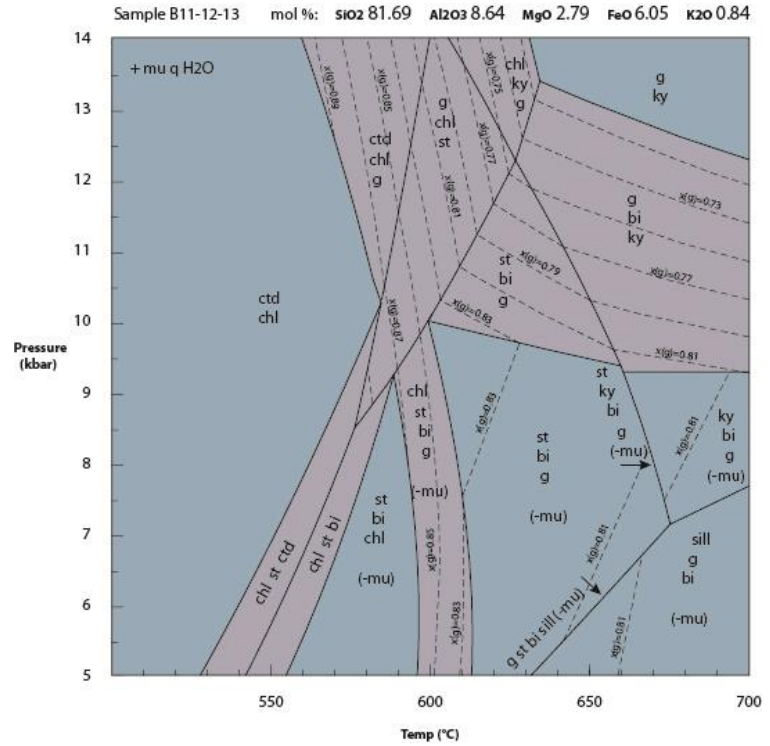


Pseudosection 1.

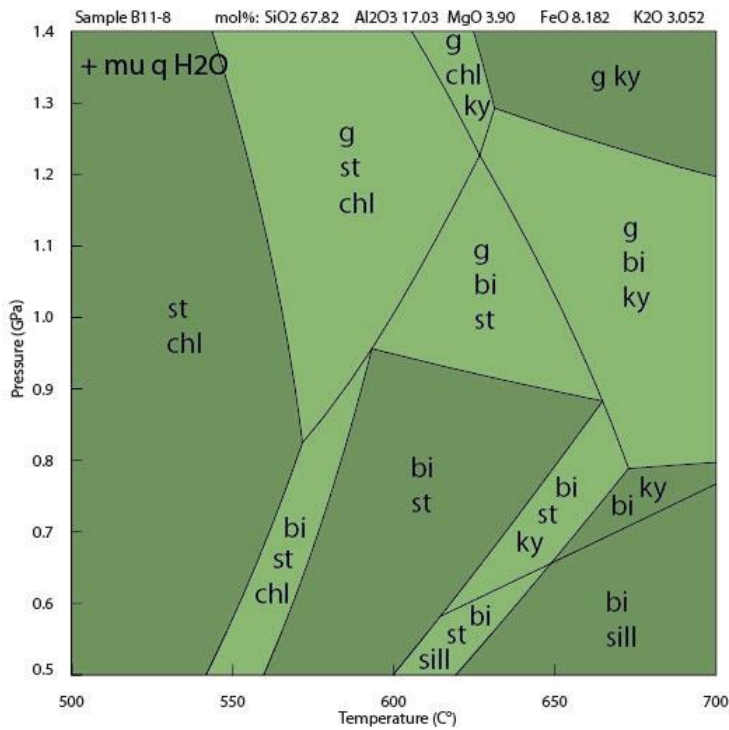


Pseudosection 2.

Isopleths for $Fe/(Fe+Mg)$ -fraction in garnet, $x(g)$, are calculated for constraining areas within the stability fields in pseudosection 1 where a P-T window can be narrowed down. This was not possible for the $Al/(Al+Mg+Fe)$ -fraction in muscovite, $y(mu)$, since muscovite presence is very limited in B11-12-13 and does not plot in any field. The pseudosection containing isopleths for garnet (pseudosection 3) can be found in larger format in appendix J. The pseudosections does not contain the desired field of only garnet, biotite and chlorite which are the only index minerals seen in the sample B11-12-13.



Pseudosection 3.



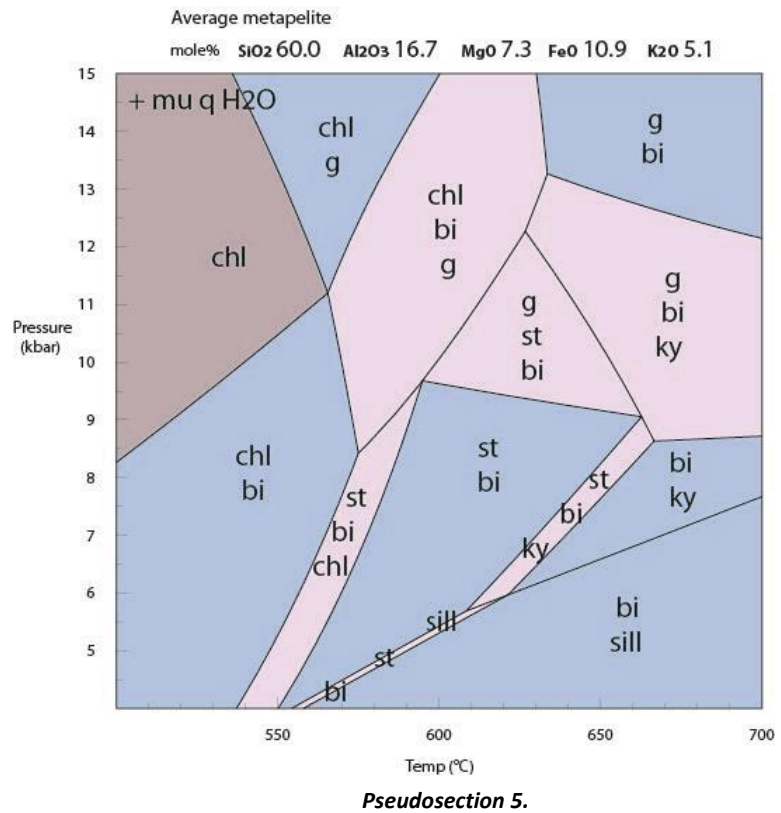
Pseudosection 4.

The pseudosections 1 and 2 were constructed from a staurolite-absent sample and made for comparison to a pseudosection of a staurolite-present sample, pseudosection 4, to see whether the different mineral assemblages seen in the thin sections would coincide at the same P-T window, assuming both samples were affected by the same P-T conditions. This comparison could not be done because the desired field of garnet, biotite and chlorite could not be calculated within the staurolite absent sample B11-12-13. Pseudosection 4 is constructed from sample B11-8 by Linde (2013). Bulk composition for pseudosection 4 can be seen in the top of the pseudosection.

Although the phase fields of B11-12-13 (pseudosection 1) and B11-8 (pseudosection 4) do not coincide, some comparisons can be done. The differences in garnet stability is one pronounced effect of the differences in bulk composition. Pseudosection 1 contains a wider pressure range of garnet stability than pseudosection 4 while the opposite can be seen in staurolite and muscovite stability fields. Pseudosection 1 requires chloritoid to stabilize three of the low grade fields. The only similarities are the high P-T fields, above ~ 600 °C and ~ 9 kbar (0.9 GPa). See Appendix G for input- and output-data for THERMOCALC 3.37.

Since the stability fields depend on the bulk composition, it is interesting to see if any larger changes would allow a field containing only chlorite, biotite and garnet as index minerals. For that reason, a comparison is made between pseudosection 1 and a pseudosection which is constructed from a bulk composition representing an average metapelite named pseudosection 5. This bulk composition is taken from Philpotts & Ague (2009) as well as the *petrogenesis course* available at the Department of Geological Sciences at Stockholm University (2013).

The differences seen between pseudosection 1 and 5 are similar to those between 1 and 4, garnet is stable at a larger pressure range in pseudosection 1 than in 4 or 5, and chloritoid stability fields as well as muscovite absent field are visible in pseudosection 1 but not in 4 or 5. In addition to these differences, the main feature in pseudosection 5 is the presence of a field containing chlorite, biotite and garnet. This generates the question; is it any one element in the bulk composition that is of greater importance for generating this field?



Except for the obvious differences in SiO_2 levels, there are also small differences in the other elements. All elements except SiO_2 has been normalized to 100 % to highlight the small differences in K_2O , MgO , FeO and Al_2O_3 . Sample B11-12-13 (pseudosection 1) is relatively enriched in FeO and Al_2O_3 while the average metapelite (pseudosection 5) is relatively enriched in MgO and K_2O . The relative differences between oxides are visualized in figure 20.

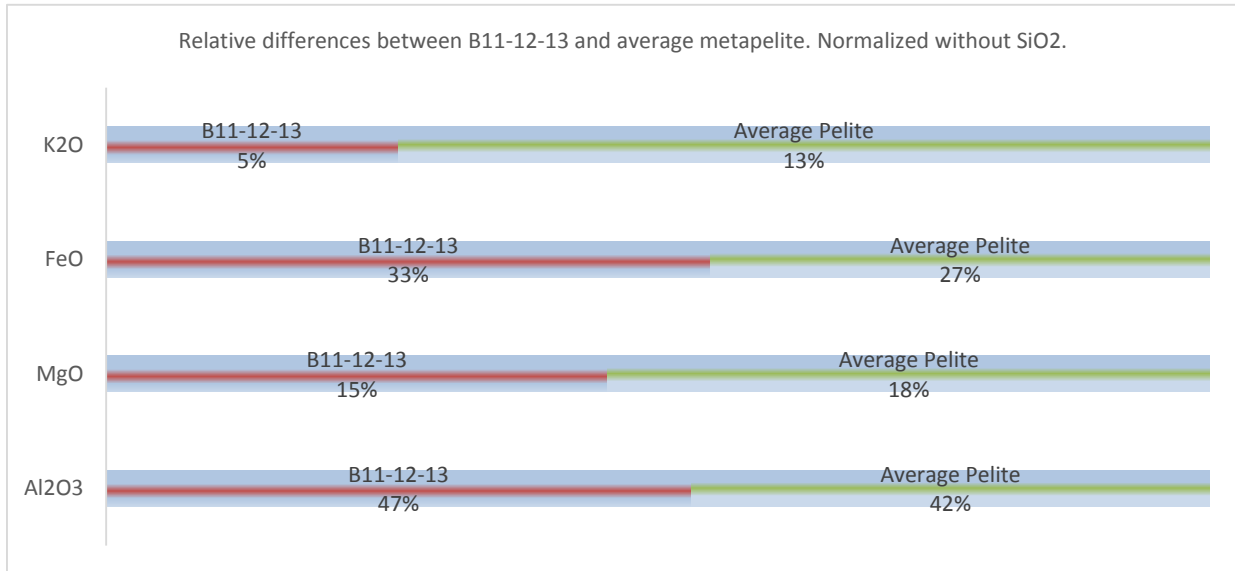


Figure 20. The differences in K_2O , FeO , MgO and Al_2O_3 between B11-12-13 and average metapelite. Oxides are normalized to 100 % without SiO_2 to highlight the differences.

Pressure- Temperature estimates

One expectation from the pseudosections was, as mentioned before, to find one field in both pseudosection 1 and 4 that represents the sample mineralogy and that coincides in roughly the same P-T-window. Since this did not work, two other methods for constraining a pressure/temperature (P-T)-window were used.

Activity acquired from AX2 based on EMP-data allowed THERMOCALC 3.33 to calculate P-T dependent fractionation of elements in minerals. For example Fe/Mg ratios in garnet and biotite as mentioned previously. Figure 21 shows the calculated pressure and temperature values. The results of THERMOCALC calculations based on activity data covers pressures from 7.4 to 11.4 kbars and temperatures from 553 to 685 °C with margin of errors, equal to standard deviations from THERMOCALC, from 6.2 to 12.7 kbars as well as 536 to 824 °C. Standard deviations (black, solid bars) show very large values and the scatter among the data points are covering a P-T window that is unreasonably large as well. These anomalies are believed to depend on disequilibrium among the phases which yield unreasonable activity. This problem could have originated while performing microprobe analysis if neighboring minerals were in disequilibrium to each other. Output data with associated reactions can be found in appendix G.

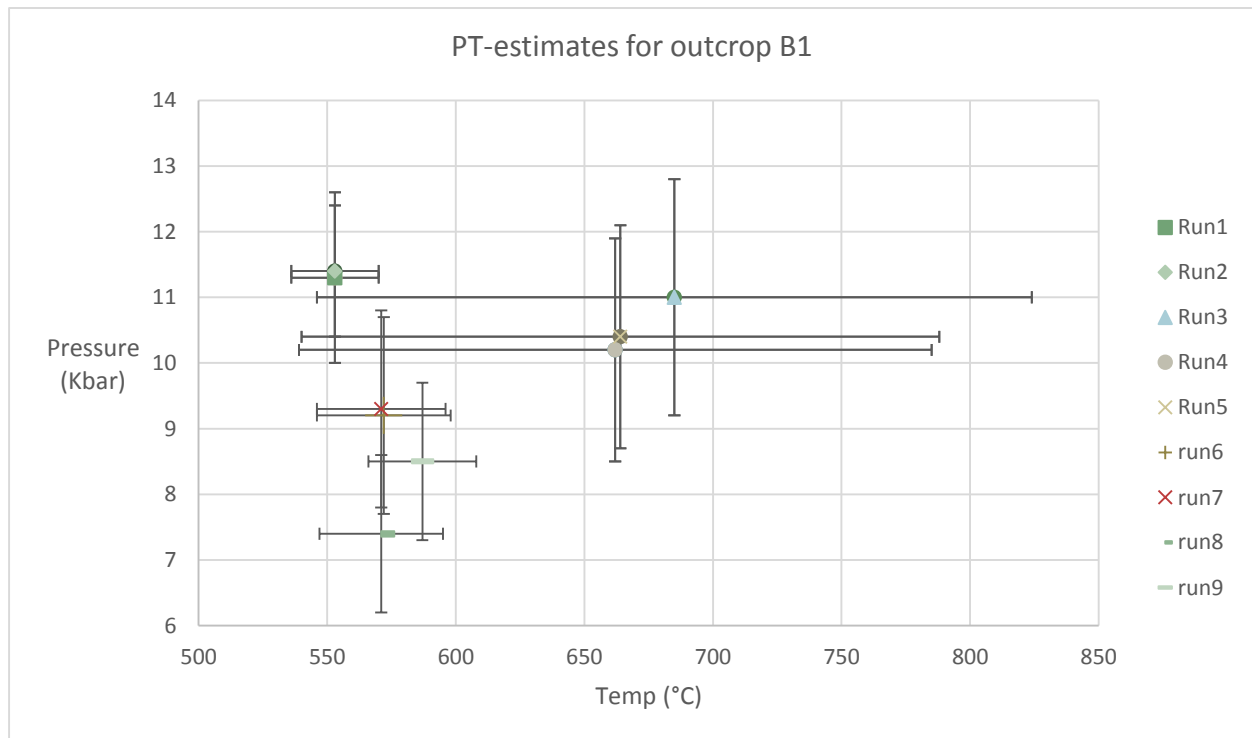


Figure 21. Graph shows pressure & temperature estimates for samples B11-10 (run: 1, 2, 6, 7, 8, 9) and B11-2-3 (run: 3, 4 and 5). Activity is calculated by AX2 and estimates are calculated by THERMOCALC 3.33.

A second way of constraining a P-T window were to calculate the partitioning of elements in garnets and muscovite respectively and present as isopleths. The isopleths were then calculated for the rock assemblage containing only chlorite, biotite and garnet; the assemblage which could not be calculated for the pseudosection. This is a way of forcing THERMOCALC to calculate isopleths in a phase field that is not allowed in a normal pseudosection. The small area where the isopleths intersect (colored area in figure 21) represents the narrowed P-T window at which the rock reached peak metamorphism.

For calculating the *Fe*-amount in garnets, as well as the fraction of its end members, a mean assemblage of all analyzed garnets were used. The result is presented as mole fraction $Fe/(Fe+Mg)$. Considering the amounts of oxides in the garnets, the mean garnet of analyzed samples is mainly almandine. All iron is calculated as *FeO*. The following table lists the mol % of garnet end members.

<i>Almandine</i>	<i>Pyrope</i>	<i>Grossular</i>	<i>Spessartine</i>
~ 78.5 %	~ 8.8 %	~ 6.7 %	~ 6.0 %

The isopleths in figure 22 represent a narrower P-T window (colored field) based on calculations of mole fractions of elements in muscovite and garnet and is plotted on the desired rock assemblage of chlorite, biotite and garnet, the actual assemblage of B11-12-13. Note that this is not a field within any pseudosection. The calculated mole fractions calculated from EMP-data are $x(\text{garnet})=0.90$ and $y(\text{muscovite})=0.89$. For EMP-data for garnets, see appendix F. For complete element fractionation of elements in muscovite, see appendix H.

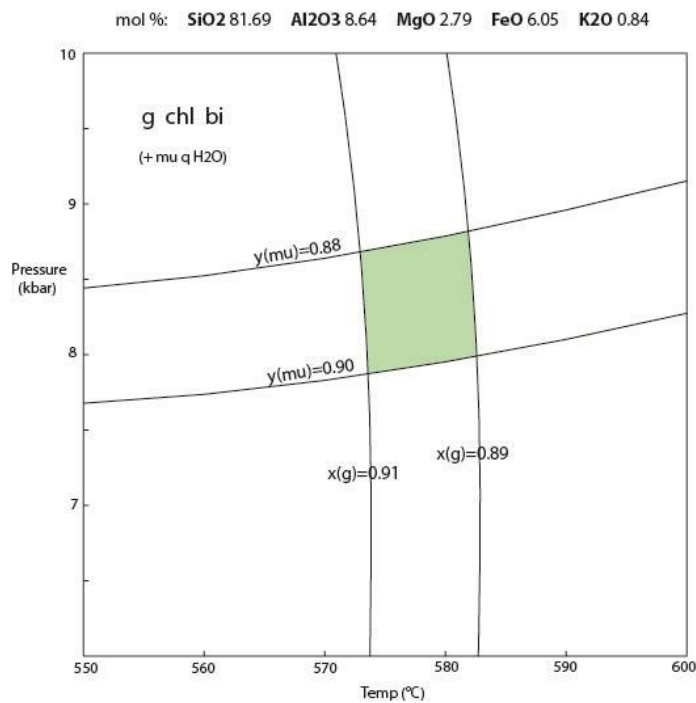


Figure 22. Graph shows isopleths for element fractions in garnet and muscovite. Partitioning values represent actual values from EMP-data and isopleths are calculated on actual mineral assemblage and bulk composition.

Discussion

At this point it is time to answer the questions stated in the aim of this thesis. Does staurolite mode increase toward the veins? If this is the case, does it depend on the interaction of fluids? To determine this, several tests were performed to determine the rock chemistry and mineralogy in combination to geothermobarometric and stoichiometric calculations. Focus has been on outcrop B1 and the profiles 1 and 2. The analyses has been performed on both staurolite present and absent samples within this profile.

Chemical and petrographic analyses

XRF-results show inverse trends of SiO_2 in relation to Al_2O_3 , FeO and K_2O while NaO amounts show similar trends as SiO_2 . The inverse trend is more pronounced in the samples where there are veins. The amounts of oxides differ overall more in the samples containing veins which indicates that the bulk rock chemistry changes in the presence of veins. In samples B11-1 to B11-3-4 no big changes can be seen, but approaching the veins, large changes in oxide distribution is visible. In samples B11-8 and B11-10 where the SiO_2 amount are corrected for the SiO_2 tied up in veins it is clear that the amount decreases, indicating that some of it has been redistributed to the veins. The vein in B11-10 contains 33 % of Na_2O , K_2O , MgO and CaO which explains the high mode of plagioclase seen in the low resolution point counting results in figure 16.

Looking at mineral modes in profile B11 it is clear that staurolite is more abundant in the areas next to the veins in contrast to chlorite which is less abundant next to the veins. It is a pronounced inverse trend among the mineral modes of staurolite and chlorite as well as garnet and chlorite. An exception to this trend can be seen in samples B11-10 to B11-12-13 where staurolite not is present. This anomaly can be correlated to the high amounts of SiO_2 and quartz seen in those samples. High amounts of quartz generally correlates to low amounts of staurolite throughout the whole profile.

Petrographic analysis, using microscope as well as backscatter electron detector, indicates that minerals have grown through both prograde and retrograde metamorphism. Garnets show increased amounts of Mn at the rims indicating prograde metamorphism (Vorhies & Ague, 2011). On the other hand, an indication of retrograde metamorphism is the almandine/pyrope-ratios seen in garnet rims in contrast to cores. EMP-data shows that this ratio is overall higher toward the garnet rims which is typical for retrograde metamorphism as garnet equilibrate chemically with bordering biotite through the exchange of Fe and Mg (Kohn, et al. 2000). Many staurolite crystals also show evidence of retrograde metamorphism as they in many cases are replaced by chlorite and muscovite.

Stoichiometry

An attempt by doing stoichiometric calculations were made to figure out if reactions would produce high amounts of quartz. If some of the reactions would produce more quartz than what is visible in the mineral mode, it would be an indication that the quartz must have gone somewhere, possibly into the vein. This was not the case since the samples generally contain higher mode of quartz than was calculated from the reactions. The excess quartz was probably already contained in the protolith since it is assumed to be derived from an oceanic shelf. It is still possible that quartz have been removed from the rock and added to an adjacent vein. Biotite mode was much lower in sample B12-6 than what was calculated. This might indicate that biotite had been consumed by some other reactions.

Figures 18 and 19 show ratios of products/reactants in a staurolite-in reaction and a garnet-in reaction, both plausible to have happened during metamorphism. The results show large differences in product/reactant ratios in two areas next to veins. These areas correlate to low amounts of SiO_2 in bulk composition compared to the area in B11-10 where both SiO_2 and quartz amounts are high. The areas in B12-4-5 show very low products/reactants ratios which correlates to relatively high amounts of quartz. Sample B12-4-5 is part of the sequence in the profile with no changes in bulk composition through ~16 cm, from sample B11-1 to B12-4-5. Reaction rates were high in two areas, one where quartz amounts are relatively low and one area where most oxide levels changes remarkably.

Pressure – Temperature estimates

Since P-T estimates yielded large scatter of values and deviations, 6.2 to 12.7 kbars and 536 to 824 °C, it is impossible to pinpoint any reasonable P-T window for peak metamorphism. The reasons for this could be the lack of phases in the calculations and that the partitioning of elements in the minerals do not represent equilibrium. The isopleths for the actual fractionation of elements in garnet and muscovite that were calculated on a stability field with the real mineral assemblage in figure 22 gave highly reasonable values of ~8.5 kbar and ~570 °C. These results are consistent with previous studies from the area in and near Glen Esk. Isopleths for garnet in pseudosection 1 did not cross any field representing the sample so these values are questionable but one area in the st, g, chl field coincide with isopleths in figure 22 at ~8.5 kbar and ~570 °C.

Pseudosections

Pseudosection 1 was constructed from the bulk composition of sample B11-12-13 which is staurolite absent. Unfortunately, THERMOCALC did not calculate any stability field containing only the identified mineral assemblage chlorite, garnet and biotite. The bulk composition does not allow such a field. According to THERMOCALC, the sample should contain staurolite as well.

Comparing the bulk compositions of B11-12-13 seen in pseudosection 1 and the average metapelite seen in pseudosection 5, the most striking difference is the SiO_2 amounts, ~81 % and 60 % respectively.

By normalizing the oxides to 100 %, disregarding SiO_2 , other differences appear clearly. B11-12-13 contains higher amounts of FeO and Al_2O_3 than the average metapelite while the opposite can be seen in K_2O and MgO . This might explain why THERMOCALC calculated large areas of Fe - and Al -bearing minerals like staurolite, chloritoid and garnet and small areas of K -bearing minerals like muscovite and biotite for pseudosection 1 compared to pseudosections 4 and 5. This is an indication that the sample is in disequilibrium and that fluids probably not were present to trigger any staurolite-in reaction.

This brings up a question regarding calculating phase fields in THERMOCALC; Are the amounts of K_2O , Feo , MgO and Al_2O_3 more, less or equally important for the mineralogy than the SiO_2 amounts? This can be answered by pitching different scenarios. If the protolith would contain only SiO_2 , the metamorphosed rock would be a quartzite containing no index minerals at all. If the protolith would contain very little or no SiO_2 the metamorphosed rock would not contain any index minerals since these minerals are silicates (Nesse, 2009). The SiO_2 amounts are therefore important. Considering that pseudosections 1 and 2 are very similar (the invariant points are in the exact same coordinates for both pseudosections) although the SiO_2 amounts differ by $\sim 6\%$, the relative amounts of other oxides must determine which phases are stable in the fields. This can be seen by comparing average metapelite (pseudosection 5) with B11-12-13 (pseudosection 1) where amounts of K_2O , Feo , MgO and Al_2O_3 differ remarkably. This means that right SiO_2 amount is a basic condition for index minerals to form but the amounts of K_2O , Feo , MgO and Al_2O_3 determine which minerals will potentially form.

After constructing pseudosections, an attempt was done to construct isopleths to constrain a narrow P-T field within the pseudosection that would indicate P-T conditions at peak metamorphism. Since the sample was staurolite absent, pressure dependent staurolite isopleths were not made. Muscovite isopleths could not be fitted to any field within the pseudosection. Garnet isopleths were made and the actual ratio of $Fe/(Fe+Mg)$ were fitted into several fields in pseudosection 3. Although the isopleths for $x(g)=0.89$ in pseudosection 3 do not exist within a field containing only garnet, chlorite and biotite one isopleth coincide with the ones in figure 22 calculated for the actual mineral assemblage. These isopleths are combined in figure 23. Assuming that P-T conditions at peak metamorphism was ~ 8.5 kbar and $\sim 570^\circ C$ as indicated from figure 22, this indicates that the sampled rock should have developed staurolite but never did. Once again, this indicates that fluids probably not were present allow any staurolite forming reaction.

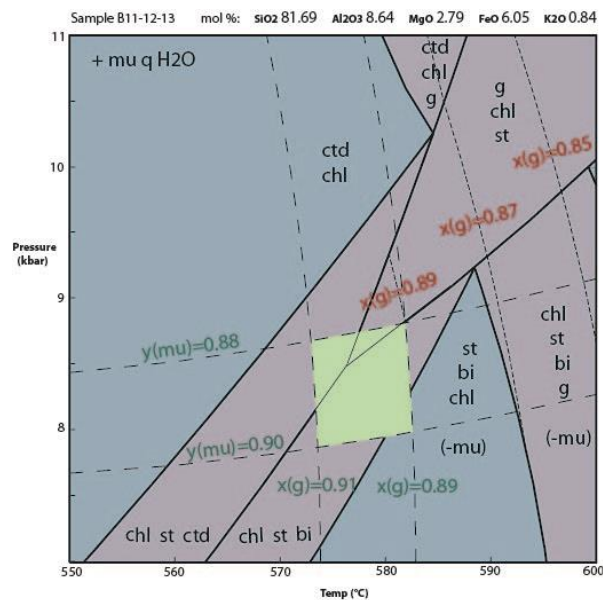


Figure 23. Isopleths representing actual mineral assemblage garnet, chlorite and biotite (from figure 22) overlain on top of phase fields from pseudosection 1 containing garnet isopleths.

Sources of uncertainty

When making two-dimensional profiles upon the outcrops, there are most likely errors because of the uneven surfaces of the rocks. These measurements are considered to be within a margin of error of <3mm, not much more than the dividing lines drawn with a permanent marker. The same margin of error is applied when sawing and polishing rocks during sample preparation because of the material loss inflicted by the sawing blade.

When calculating P-T conditions and mineral phases, assumptions are made that the mineral phases are in equilibrium to each other and that the bulk composition is representative for the pelitic part of the rock. Regarding the pseudosections and P-T estimates it is not certain that the mineral phases were in equilibrium. This could be seen as pseudosection 1 did not contain the desired field representing the mineral phases seen in the thin section. P-T estimates yielded very large standard deviations. This is probably also due to disequilibrium.

Conclusion

Staurolite mode depends on bulk composition and fluid interaction as well as pressure and temperature during metamorphism. Results presented in this study support the fact that staurolite mainly forms within selvages adjacent to quartz veins. This happens as fluids flow through cracks during quartz vein formation, redistributes elements and changes the bulk rock composition by diffusion within the rock, favoring nucleation and growth of staurolite. The rock sampled in the staurolite zone in Glen Esk reached peak pressure of ~8.5 kbar and peak temperature of ~570 °C during metamorphism.

Acknowledgements

I would like to express my gratitude to my supervisors Alasdair Skelton and Alexander Lewerentz for devising this project and its working methods. Big thanks to Dan Zetterberg, Runa Jacobsson and Jaroslaw Majka for helping out with the analyses. And last but not least, Thanks to Josefin Linde for good discussions and for being a great coworker.

References

Articles & Research abstracts:

- Ague J. J., *Extreme channelization of fluid and the problem of element mobility during Barrovian metamorphism*, American Mineralogist, vol. 96, (2011), pp 333 – 352
- Alvarez M., *Glass Disk Fusion Method for the X-Ray Fluorescence Analysis of Rocks and Silicate*, X-Ray Spectrometry Vol. 19, (1990) 203 – 206
- Baker A. J., *Pressures and temperatures of metamorphism in the eastern Dalradian*, Journal of the Geological Society, vol. 142 (1985), pp 137 - 148
- Barrow G., *On the geology of lower dee-side and the southern highland border*, Proceedings of the Geologists' Association, Volume 23, Issue 5, (1912), Pages 274-290
- Dewey J. F., *Orogeny can be very short*, National Academy of Sciences (1997)
- Ferry J. M., *A historical review of metamorphic fluid flow*, Journal of geophysical research, vol. 99, B5, (1994), pp 15,487 – 15,498
- Ferry J. M., Spear F. S., *Experimental Calibration of the Partitioning of Fe and Mg Between Biotite and Garnet*, Contributions to Mineralogy and Petrology, nr 66, Springer-Verlag, (1978), pp 113 - 117
- Fettes D. J., Macdonald R., Fitton J. G., Stephenson D., Cooper M. R., *Geochemical evolution of Dalradian metavolcanic rocks: implications for the break-up of Rodinia supercontinent*, Journal of the Geological Society, 168 (2011), pp 1133 - 1146
- Hoisch T. D., *Empirical calibration of six geobarometers for the mineral assemblage quartz+muscovite+biotite+plagioclase+garnet*, Contributions to Mineralogy and Petrology, 104, Springer-Verlag (1990), 225 - 234
- Holland T.J.B., Baker J.M., Powell R., *Mixing properties and activity-composition relationships of chlorites in the system MgO-FeO-Al₂O₃-SiO₂-H₂O*, European Journal of Mineralogy, 10 (1998), 395-406.
- Holland T.J.B., Powell R., *An internally consistent thermodynamic dataset for phases of petrological interest*. Journal of Metamorphic Geology, 16 (1998a), 309-343.
- Kohn M. J., Spear F., *Retrograde net transfer reaction insurance for pressure-temperature estimates*, Geology, 28, Geological Society of America (2000) pp 1127 – 1130
- Kozoil A. M., Newton R. C., *Redetermination of the anorthite breakdown reaction and improvement of the plagioclase-garnet-Al₂SiO₅-quartz geobarometer*, American Mineralogist, vol. 73 (1988), 216 – 223
- Lewerentz A., Skelton A., Möller C., Crill P., *Vein controlled stabilisation of Barrovian index minerals: observations from Glen Esk*, Abstract, 31st Nordic Geological winter meeting, Lund (2014)
- Linde J., *Increased Staurolite mode due to selvage formation in the Staurolite zone of Glen Esk, Scotland*, Masters Thesis, Department of Geological Sciences, Stockholm University (2013)
- Lyubetskaya T., Ague J. J., *Modeling the Magnitudes and Directions of Regional Metamorphic Fluid Flow in Collisional Orogens*, Journal of Petrology, vol. 30, nr. 8, (2009), pp 1505 – 1531
- Nabelek P. I., *Quartz-sillimanite leucosomes in high-grade schists Black Hills, South Dakota: A perspective on the mobility of Al in high-grade metamorphic rocks*, Geology (1997), 995 - 998
- Pettersson R. P., Selin-Lindgren E., *Energy-dispersive X-Ray fluorescence analysis*, Surface Characterization: A User's Sourcebook, Chapter 8, WILEY-VHC Verlag, (1997)
- Powell R., Holland T., Worley B., *Calculating phase diagrams involving solid solutions via non-linear equations, with examples using THERMOCALC*, Journal of metamorphic Geology, nr 16, (1998), pp 577 – 588
- Skelton A. D. L., *The effect of metamorphic fluid flow on the nucleation and growth of garnets in Troms, North Norway*, Journal of Metamorphic Geology, 15 (1997), pp 85 – 92
- Stephenson D., Mendum J. R., Fettes D. J., Leslie A. G., *The Dalradian rocks of Scotland: an introduction*, Proceedings of the Geologists Association 124, (2013), 3 – 82
- Tanner G.P.W., Thomas C. W., Harris A.L., Gould D., Harte B., Treagus J. E., Stephenson D., *The Dalradian rocks of the Highland Border region of Scotland*, Proceedings of the Geologists Association 124, (2013), 215 – 262

- Tilley C. E., *A Preliminary Survey of Metamorphic Zones in the Southern Highlands of Scotland*, Quarterly Journal of the Geological Society, vol. 81, (1925), pp 100 - 112
- Vorhies S. A., Ague J. J., *Pressure–temperature evolution and thermal regimes in the Barrovian zones, Scotland*, Journal of the Geological society, London, Vol. 168, (2011), pp. 1147 – 1166
- Walther J. V., *Fluid – Rock Reactions during Metamorphism at Mid-Crustal Conditions*. The Kournal of Geology, vol. 102, No. 5, (1994), pp 559 – 570
- White R.W., Powell R., Holland T.J.B., *Progress relating to calculation of partial melting equilibria for metapelites*. Journal of Metamorphic Geology, 25 (2007), 511-527.

Literature:

- Winter J. D., *Principles of Igneous and Metamorphic Petrology*, 2nd Ed., International Ed., Pearson, New Jersey, USA, (2010), pp 139, 140, 238, 572, 583, 587
- Philpotts A. R., Ague J. J., *Principles of Igneous and Metamorphic Petrology*, Cambridge University press, Cambridge, (2009), pp 483
- Nesse W. D., *Introduction to mineralogy*, Oxford University press, Oxford, (2009), Chapters 12, 13, 16

Internet sources:

- <http://www.webmineral.com> (2013-12-04)
- <http://www.tellus.geo.su.se/petrogenesis/index.html> (2013-12-09)
- www.westscotland.com (2013-12-11)
- www.geologyrocks.co.uk (2013-12-11)

Appendix

A Loss on ignition

Loss on ignition results

Sample	Crucible weight (gram)	Sample weight (gram)	Crucible + Sample weight (gram)	After 105 °C weight (gram)	LOI dif. 105 °C	After 1000 °C weight (gram)	LOI dif. 1000 °C
B11-1	23,63	5,07	28,70	28,69	0,01	28,56	0,13
B11-2-3	22,85	4,95	27,80	27,80	0,00	27,70	0,10
B11-3-4	24,09	4,92	29,01	29,01	0,00	28,91	0,10
B11-5	22,98	5,03	28,01	28,01	0,00	27,94	0,08
B11-8	22,75	5,02	27,77	27,77	0,00	27,67	0,10
B11-9	25,40	5,01	30,41	30,41	0,00	30,36	0,05
B11-10	24,55	5,02	29,57	29,56	0,01	29,46	0,11
B11-10p	24,07	5,04	29,12	29,11	0,00	29,03	0,08
B11-10q	23,64	5,00	28,64	28,64	0,00	28,63	0,01
B11-11	25,36	5,05	30,41	30,42	-0,01	30,39	0,03
B11-12-13	23,05	5,00	28,04	28,04	0,00	28,01	0,03
B21-9	23,04	5,11	28,15	28,15	0,01	28,07	0,09
B21-8-9	23,39	4,68	28,07	28,06	0,01	27,92	0,16
B21-10	22,72	5,31	28,03	28,02	0,01	27,88	0,15
B21-11	23,02	5,86	28,88	28,87	0,01	28,77	0,11
B21-12	24,55	4,86	29,40	29,40	0,01	29,29	0,12
B12-3-4	24,93	4,95	29,87	29,87	0,00	29,83	0,04
B12-4-5	22,87	5,75	28,62	28,17	0,44	28,12	0,50
B12-6	23,89	4,99	28,88	28,87	0,00	28,78	0,10
B31-1	23,24	5,14	28,38	28,38	0,01	28,22	0,17
B31-2	23,37	5,25	28,62	28,61	0,01	28,46	0,16
B31-3	22,56	4,64	27,20	27,19	0,01	27,06	0,14
B41-0-1	22,91	5,00	27,91	27,91	0,00	27,79	0,12
B41-1	23,64	4,96	28,60	28,60	0,00	28,48	0,12
B41-2	25,61	4,98	30,58	30,63	-0,05	30,51	0,07
B41-3	24,30	5,58	29,87	29,86	0,01	29,74	0,13
B41-4	25,27	5,04	30,31	30,30	0,00	30,19	0,12
B41-5	25,50	5,08	30,58	30,58	0,00	30,47	0,11
B41-6	24,31	4,95	29,26	29,25	0,01	29,15	0,11
A1-1	23,52	5,03	28,56	28,56	0,00	28,46	0,10
A1-2	25,23	5,64	30,87	30,87	0,00	30,77	0,11
A1-3	24,03	5,86	29,89	29,88	0,01	29,84	0,05

B *Sample preparation*

Samples were cut with Diamond sawing blade; model *MD 120 C* by *Norton*. Samples cut for thin sections were made to a size of about 35x20x12 mm.

Milling was done in a *Retsch RS 200* machine with milling cup of 'special steel' (*Retsch*), maximum 100 ml, and run at 700 rpm at about 30 seconds.

Polishing of rock samples was made with *Silicon Carbide abrasive, size 180 (sieve)*.

C *Glass disk construction*

Glass Disks for XRF were made of powdered samples that had gone through LOI mixed with a Flux.

- 2 grams of sample
- 5 grams of Flux (66 % Lithiumtetraborat, 34 % Lithiummetaborat)

Glass fusion was made using *PHOENIX WD 400* by *XRF Scientific Ltd*.

D *XRF, technical details and data*

XRF Technical information

Machine: *Rigaku ZSX Primus II*

Calibrated every 6th run with standard disk (AGV-2) and expected standard values of (mass %):

	<i>SiO₂</i>	<i>Al₂O₃</i>	<i>CaO</i>	<i>MgO</i>	<i>MnO</i>	<i>P₂O₅</i>	<i>Fe₂O₃</i>	<i>Na₂O</i>	<i>K₂O</i>	<i>TiO₂</i>
	60.15	17.15	5.27	1.82	0.10	0.49	6.79	4.25	2.92	1.07
Std:	0.00	0.00	0.01	0.02	0.02	0.39	0.00	0.00	0.01	0.01

Raw data Outcrop B1

Outcrops: B,1,1-1 B,1,1-2-3 B,1,1-3-4 B,1,1-5 B,1,1-8 B,1,1-9

Oxides Mass%:

SiO2	59,23	57,71	58,61	58,44	54,45	71,64
Al2O3	20,79	20,74	20,33	19,34	24,77	13,85
CaO	0,94	0,79	0,89	1,53	1,29	1,30
MgO	2,96	2,94	2,77	2,87	2,10	1,61
MnO	0,07	0,15	0,18	0,11	0,28	0,08
P2O5	0,18	0,07	0,14	0,08	0,07	0,05
Fe2O3	8,93	11,36	10,70	10,69	9,56	6,57
Na2O	1,50	1,15	1,17	2,49	2,19	2,32
K2O	4,41	4,03	4,16	3,41	3,84	2,04
TiO2	1,00	1,07	1,06	1,05	1,45	0,55
Total:	100,00	100,00	100,00	100,00	100,00	100,00

Outcrops: B,1,1-9 B,1,1-10 B,1,1-11-12 B,1,1-12-13 B,1,1-10qz B,1,1-10p

Oxides Mass%:

SiO2	71,64	63,62	73,82	71,43	94,91	55,63
Al2O3	13,85	17,87	12,32	13,35	2,72	23,23
CaO	1,30	2,29	2,53	2,94	0,47	2,35
MgO	1,61	2,16	1,44	1,61	0,06	2,41
MnO	0,08	0,08	0,13	0,16	0,01	0,10
P2O5	0,05	0,05	0,04	0,04	0,00	0,05
Fe2O3	6,57	7,21	5,55	5,97	0,93	7,72
Na2O	2,32	4,16	2,66	2,80	0,69	5,31
K2O	2,04	1,67	0,99	1,13	0,19	2,18
TiO2	0,55	0,89	0,51	0,55	0,03	1,02
Total:	100,00	100,00	100,00	100,00	100,00	100,00

Outcrops: B,1,2-3-4 B,1,2-4-5 B,1,2-6

Oxides Mass%:

SiO2	67,71	58,25	65,41
Al2O3	16,03	18,10	18,08
CaO	2,62	1,95	1,11
MgO	1,61	2,89	2,13
MnO	0,08	0,18	0,06
P2O5	0,07	0,06	0,06
Fe2O3	5,28	11,93	7,20
Na2O	4,47	3,02	2,19
K2O	1,29	2,65	2,84
TiO2	0,85	0,98	0,92
Total:	100,00	100,00	100,00

E Petrographic data

Microscope used at petrographic analysis/point counting are *Leica DM LSP* and *Nikon Optiphot2* with point counting machines *Swift* model *F* and *Stepping Stage*.

Point count data Outcrop B1

Length (cm)	0-3	4-7	5-8	9-12	13-16	18-21	21-24	24-27	27-30	31-34	34-37
Sample / Thin section	B11-1	B11-2-3	B11-3-4	B11-5	B12-4-5	B12-6	B11-8	B11-9	B11-10	B11-11-12	B11-12-13
Quartz	36,3	30,4	34,4	54,8	46,2	27,8	39,2	61,3	56,4	76	74,2
Biotite	44,4	36,9	41,9	33,8	36	27	32,3	28,7	22,6	12	17,9
Muscovite	11,9	20,8	9	1,7	5,4	17,7	13,3	3,1	8,3	3,1	1
Chlorite	2,7	3,3	2,5	0,3	1	3,8	1,5	0,6	0,6	0	0,9
Plag	0,2	0	0,5	0,7	1,4	1	6,5	1,8	4,4	5	2,2
Garnet	1,7	2,3	7,2	7,4	3,3	5,8	4,1	3,2	6,3	3	3,2
Staurolite	1,5	5,6	4,5	0,6	4,6	15,5	1,6	1,3	0,2	0	0
Oxides	1,3	0,7	0	0,7	2,1	1,4	1,5	0	1,2	0,8	0,6
Total:	100	100	100	100	100	100	100	100	100	99,9	100
Qz vein (%)					10	10	5		35		

Pointcount data Outcrop B1, higher resolution

Length interval	13-16 cm										
Sample:	B1245										
Section	1	2	3	4	5	6	7	8	9	vein	10
Quartz	23,4	29	26	35,2	22,2	29,2	18,9	31	33,7		41,4
Biotite	35,9	29	40	26,4	36,1	30,4	44,5	21,6	16,8		18,5
Muscovite	10,9	22,5	11	20,5	19,4	14,6	24,3	22,9	15,5		20
Chlorite	1,5	2,8	2,8	1,4	4,1	4,8	5,4	5,4			1,4
Plag	6,2		2,8		1,3		4	4	3,8		2,8
Garnet	12,5	6,4	7,2	11,7	4,1	9,7	1,3	5,4	6,4		14,2
Staurolite	9,3	8	8,6	4,4	12,5	4,8		6,7	23,3		
Oxides		3,2				6	1,3	2,7			1,4
Qz vein (%)											10

Length interval 18-21
cm

Sample: B126

Section	1	2	3	4	5	6	7	vein	8	9	vein	10
Quartz	53,7	54	54,2	51,5	46,3	37,8	48,2		38,2	51,8		39
Biotite	37,5	37	34	40,2	50,5	42,1	35,2		26,4	39,5		19,5
Muscovite		2	1	2		5,2	2,3		6,7			10,3
Chlorite			2,1	2		1	2,3		1,1			2,2
Plag		5	3,1	2		5,2	9,4		2,2			
Garnet	6,2				2,1	3,1	1,1		7,8			3,4
Staurolite									10,1	8,6		25,2
Oxides	2,5	2	5,3	2	1	5,2	1,1		6,7			
Qz vein (%)								5			10	

Length interval 21-24
cm

Sample: B118

Section	vein	1	2	3	4	5	6	7	8	9	10
Quartz		7,4	7	14,2	8,4	5,3	22,2	57,1	61,8	61,2	59,7
Biotite		55,3	50,5	47,2	56,8	56,3	38,8	29,6	29,8	37,7	31,5
Muscovite		6,3	12,9	14,2	18,9	22,3	8,8		1		1
Chlorite		3,1		2,1	4,2	3,1	1,1	7,6	6,1	1	1
Plag		4,2	2,3	1	2,1	2,1	4,4	3,2			
Garnet		1	11,7	6,5	2,1	4,2	23,3	2,1	1		5,4
Staurolite		18	12,9	10,9	4,2	5,3					1
Oxides		4,2	2,3	3,2	3,1	1	1,1				
Qz vein (%)	5										

Length interval 24-27
cm

Sample: B119

Section	1	2	3	4	5	6	7	8	9	10
Quartz	80	53,1	63	66,6	53,8	49	64	53	42,5	51
Biotite	13,3	29,6	29,2	31,4	25,2	29,4	23,4	28,5	44,6	32,6
Muscovite	1,6	7,8	1,5	1,9	5,4	9,8	4	8,1	5,3	6,5
Chlorite		1,5	1,5				1	1	1	
Plag		3,1	1,5		2,1	2,9	2	2	3,1	
Garnet	5	3,1	1,5		3,2	4,4	4	4	1	3,2
Staurolite			1,5		9,8	1,9		3		4,3
Oxides		1,5				1,9	2		2,1	2,1
Qz vein (%)										

Length interval	27-30 cm				
Sample:	B1110				
Section	1	2	3	4	5 vein
Quartz	78,1	75	60,4	59,2	62,5
Biotite	18,1	15,3	29,1	25,9	25
Muscovite			4,1	3,7	
Chlorite					
Plag		3,8	4,1	3,7	7,5
Garnet	1,8	3,8		3,7	5
Staurolite	1,8				
Oxides		1,9	2	3,7	
Qz vein (%)	70				

F EMP-data for garnets and muscovites

EMP-data for garnets in fractionation for isopleths and Mn-levels

No.	94	95	96	14	15
F	0,00	0,00	0,00	0,00	0,00
Na2O	0,03	0,03	0,06	0,01	0,07
SiO2	37,86	37,76	38,16	37,90	37,64
Al2O3	21,43	21,66	21,36	20,52	20,59
MgO	2,13	2,50	2,27	2,48	2,47
CaO	3,48	1,64	1,69	2,27	1,66
MnO	3,56	1,45	1,40	1,54	0,57
K2O	0,00	0,02	0,05	0,00	0,04
TiO2	0,09	0,00	0,04	0,07	0,08
FeO	32,63	36,62	35,69	35,20	36,93
Cr2O3	0,03	0,04	0,03	0,01	0,03
Cl	0,00	0,00	0,00	0,00	0,02
Y2O3	0,00	0,00	0,00	0,04	0,09
NiO	0,00	0,00	0,00	0,07	0,00
Total	101,25	101,72	100,74	100,11	100,19
Comment	B1110-gt-core	B1110-gt-rim1	B1110-gt-rim2	B111-gt-core1	B111-gt-rim
No.	123	124	75	76	28
F	0,00	0,00	0,00	0,00	0,00
Na2O	0,07	0,02	0,04	0,00	0,04
SiO2	37,51	37,75	37,33	37,83	37,98

Al2O3	20,72	20,72	19,70	20,51	20,42
MgO	1,31	2,82	1,10	2,57	1,30
CaO	2,87	1,80	4,39	1,64	2,89
MnO	7,08	0,35	7,90	1,07	7,21
K2O	0,00	0,02	0,00	0,02	0,02
TiO2	0,10	0,01	0,20	0,02	0,06
FeO	31,13	37,07	27,25	35,96	30,80
Cr2O3	0,00	0,04	0,00	0,03	0,00
Cl	0,00	0,01	0,01	0,00	0,00
Y2O3	0,33	0,21	0,00	0,28	0,09
NiO	0,00	0,00	0,01	0,00	0,00
Total	101,12	100,81	97,94	99,93	100,81
Comment	B1123-gt-core	B1123-gt-rim	B118-gt-core	B118-gt-rim	B1234-gt-core

No.	36	27	35
F	0,00	0,00	0,00
Na2O	0,00	0,04	0,03
SiO2	37,24	37,73	37,76
Al2O3	20,52	20,63	20,33
MgO	2,00	2,72	2,51
CaO	2,39	1,61	1,52
MnO	1,23	0,31	0,39
K2O	0,00	0,04	0,05
TiO2	0,06	0,05	0,04
FeO	36,52	36,83	37,22
Cr2O3	0,06	0,04	0,05
Cl	0,00	0,00	0,01
Y2O3	0,06	0,01	0,11
NiO	0,02	0,00	0,03
Total	100,11	100,01	100,05
Comment	B1234-gt-core	B1234-gt-rim	B1234-gt-rim

EMP-data for muscovite used in mu-fractionation for isopleths

No.	F	Na2O	SiO2	Al2O3	MgO	CaO	MnO	K2O	TiO2	FeO	Cr2O3	Cl	Y2O3	NiO	Total	Comment
8	0	1,59	46,52	36,40	0,51	0,03	0,02	8,79	0,35	1,06	0	0	0	0	95,23	A12-mu1
9	0	1,64	46,58	36,09	0,56	0,03	0,03	8,76	0,41	0,97	0	0	0	0	95,06	A12-mu2
Average:	0	1,61	46,55	36,25	0,53	0,03	0,03	8,78	0,38	0,95	0	0	0	0		

Machine: JEOL model JXA 8530F, Dpt. of Earth Sciences, Uppsala University

Software: THERMOCALC 3.33, 3.37 and AX2 by Holland & Powell

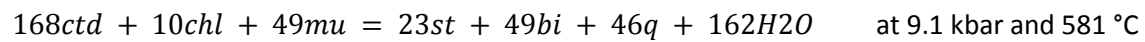
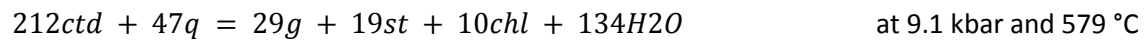
Output data for P-T estimates

<p>Sample B11-10</p> <p><u>run 1</u></p> <p>Independent set of reactions</p> <ol style="list-style-type: none"> 1) $3\text{ames} + \text{py} + 2\text{gr} + 6\text{q} = 6\text{an} + 3\text{clin}$ 2) $15\text{ames} + 10\text{gr} + 5\text{alm} + 30\text{q} = 30\text{an} + 12\text{clin} + 3\text{daph}$ 3) $\text{py} + 2\text{gr} + 3\text{east} + 6\text{q} = 6\text{an} + 3\text{phl}$ 4) $3\text{clin} + 5\text{ann} = 3\text{daph} + 5\text{phl}$ 5) $12\text{an} + 2\text{clin} + 5\text{ann} = 4\text{gr} + 5\text{alm} + 5\text{east} + 8\text{q} + 8\text{H}_2\text{O}$ <p>T = 553jC, sd = 17, P = 11.3 kbars, sd = 1.3, cor = -0.381, sigfit = 0.51</p>		<p><u>run 2</u></p> <p>Independent set of reactions</p> <ol style="list-style-type: none"> 1) $3\text{ames} + \text{py} + 2\text{gr} + 6\text{q} = 6\text{an} + 3\text{clin}$ 2) $15\text{ames} + 10\text{gr} + 5\text{alm} + 30\text{q} = 30\text{an} + 12\text{clin} + 3\text{daph}$ 3) $\text{py} + 2\text{gr} + 3\text{east} + 6\text{q} = 6\text{an} + 3\text{phl}$ 4) $3\text{clin} + 5\text{ann} = 3\text{daph} + 5\text{phl}$ 5) $12\text{an} + 2\text{clin} + 5\text{ann} = 4\text{gr} + 5\text{alm} + 5\text{east} + 8\text{q} + 8\text{H}_2\text{O}$ <p>T = 553jC, sd = 17, P = 11.4 kbars, sd = 1.3, cor = -0.382, sigfit = 0.51</p>	
<p>Sample B11-2-3</p> <p><u>run3</u></p> <p>Independent set of reactions</p> <ol style="list-style-type: none"> 1) $3\text{east} + 6\text{q} = \text{phl} + \text{py} + 2\text{mu}$ 2) $\text{phl} + \text{east} + 6\text{q} = \text{py} + 2\text{cel}$ 3) $2\text{ann} + \text{mu} + 6\text{q} = \text{alm} + 3\text{fcel}$ 4) $\text{phl} + 2\text{ann} + 3\text{east} + 18\text{q} = 3\text{py} + 6\text{fcel}$ <p>T = 685jC, sd = 139, P = 11.0 kbars, sd = 1.8, cor = 0.132, sigfit = 1.25</p>	<p>OBS! Staurolite present!</p>	<p><u>run4</u></p> <p>Independent set of reactions</p> <ol style="list-style-type: none"> 1) $3\text{east} + 6\text{q} = \text{phl} + \text{py} + 2\text{mu}$ 2) $\text{phl} + \text{east} + 6\text{q} = \text{py} + 2\text{cel}$ 3) $2\text{ann} + \text{mu} + 6\text{q} = \text{alm} + 3\text{fcel}$ 4) $\text{phl} + 2\text{ann} + 3\text{east} + 18\text{q} = 3\text{py} + 6\text{fcel}$ <p>T = 662jC, sd = 123, P = 10.2 kbars, sd = 1.7, cor = 0.109, sigfit = 1.12</p>	<p><u>run5</u></p> <p>Independent set of reactions</p> <ol style="list-style-type: none"> 1) $3\text{east} + 6\text{q} = \text{phl} + \text{py} + 2\text{mu}$ 2) $\text{phl} + \text{east} + 6\text{q} = \text{py} + 2\text{cel}$ 3) $2\text{ann} + \text{mu} + 6\text{q} = \text{alm} + 3\text{fcel}$ 4) $\text{phl} + 2\text{ann} + 3\text{east} + 18\text{q} = 3\text{py} + 6\text{fcel}$ <p>T = 664jC, sd = 124, P = 10.4 kbars, sd = 1.7, cor = 0.113, sigfit = 1.13</p>

Run 6, 7, 8 and 9 are taken from Linde (2013).

Stoichiometry of staurolite-in reaction:	kbar:	°C:
% 48g + 12chl + 68mu = 10st + 68bi + 144q + 28H ₂ O	6.500	521.08
% 44g + 15chl + 67mu = 10st + 67bi + 136q + 40H ₂ O	7.000	540.43
% 39g + 18chl + 65mu = 10st + 65bi + 126q + 51H ₂ O	7.500	555.05
% 34g + 20chl + 64mu = 10st + 64bi + 117q + 60H ₂ O	8.000	566.68
% 31g + 22chl + 63mu = 10st + 63bi + 109q + 68H ₂ O	8.500	576.37
% 28g + 23chl + 62mu = 10st + 62bi + 104q + 74H ₂ O	9.000	584.78
% 26g + 24chl + 61mu = 10st + 61bi + 100q + 78H ₂ O	9.500	592.32
% 25g + 25chl + 61mu = 10st + 61bi + 97q + 81H ₂ O	10.000	599.26
% 24g + 26chl + 61mu = 10st + 61bi + 96q + 83H ₂ O	10.500	605.77
% 24g + 26chl + 61mu = 10st + 61bi + 95q + 84H ₂ O	11.000	611.97
% 24g + 26chl + 61mu = 10st + 61bi + 95q + 85H ₂ O	11.500	617.92
% 23g + 26chl + 61mu = 10st + 61bi + 95q + 86H ₂ O	12.000	623.67
% 23g + 27chl + 61mu = 10st + 61bi + 95q + 86H ₂ O	12.500	629.28
% 23g + 27chl + 61mu = 10st + 61bi + 96q + 86H ₂ O	13.000	634.76
% 23g + 27chl + 62mu = 10st + 62bi + 96q + 87H ₂ O	13.500	640.13
% 23g + 27chl + 62mu = 10st + 62bi + 97q + 87H ₂ O	14.000	645.40
% 23g + 27chl + 62mu = 10st + 62bi + 98q + 87H ₂ O	14.500	650.58
% 23g + 27chl + 63mu = 10st + 63bi + 99q + 88H ₂ O	15.000	655.68

Other staurolite –in reactions that were considered, but not pursued, for stoichiometric tests:



H Fractionation of elements in muscovite

The mole fraction of mean muscovite in staurolite absent rock in outcrop A1 follows below. Calculations are based on EMP-data.

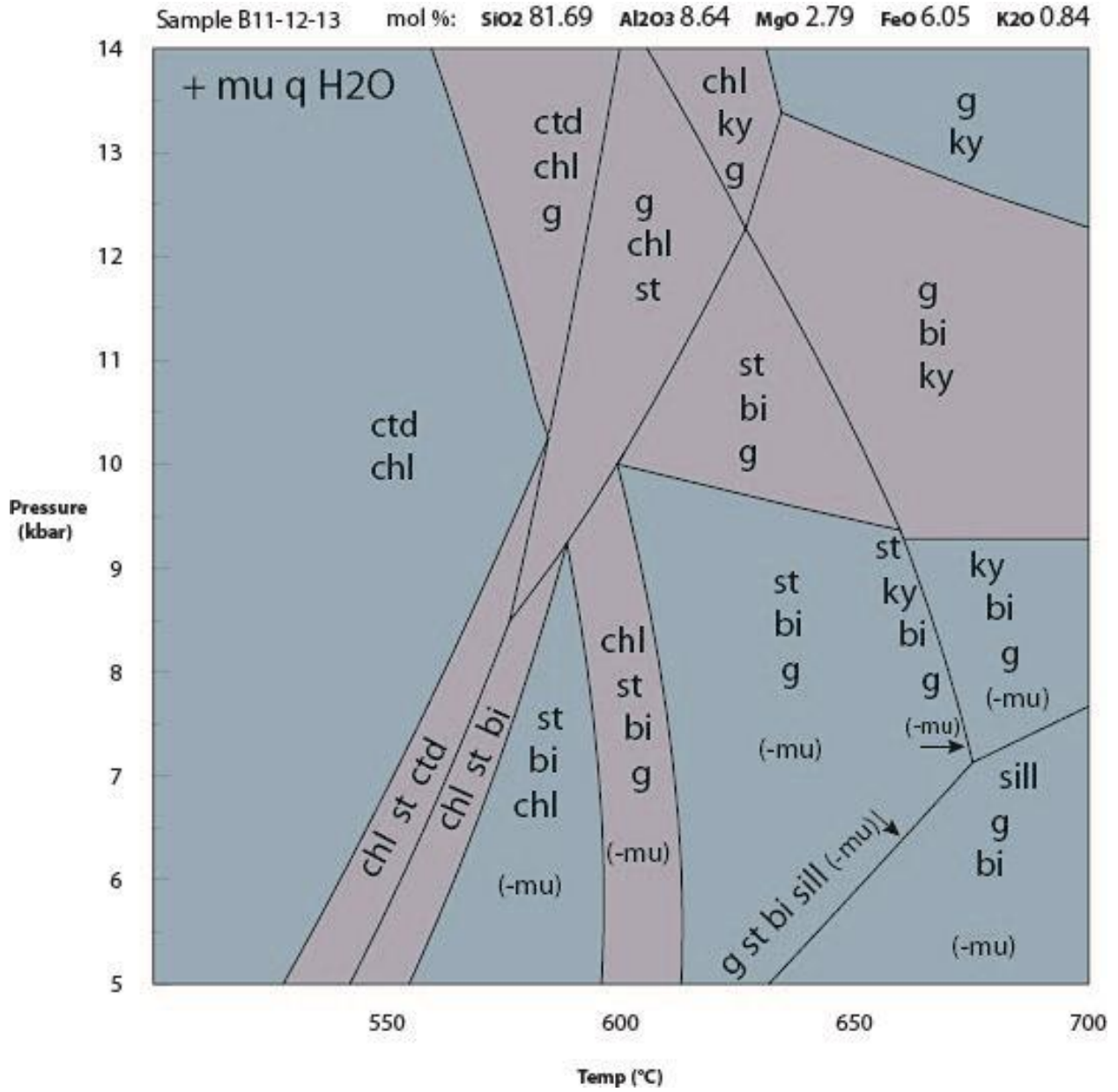
Position:	(1 st geometric structure – M2)		(2 nd geometric structure)			
	1	2	1	2	3	4
Al (mole fraction):	0.89	1	0.93	0	0	0
Si (mole fraction):	0	0	0.07	1	1	1
Mg (mole fraction):	0.05	0				
Fe (mole fraction):	0.06	0				

I Abbreviations and chemical formulas

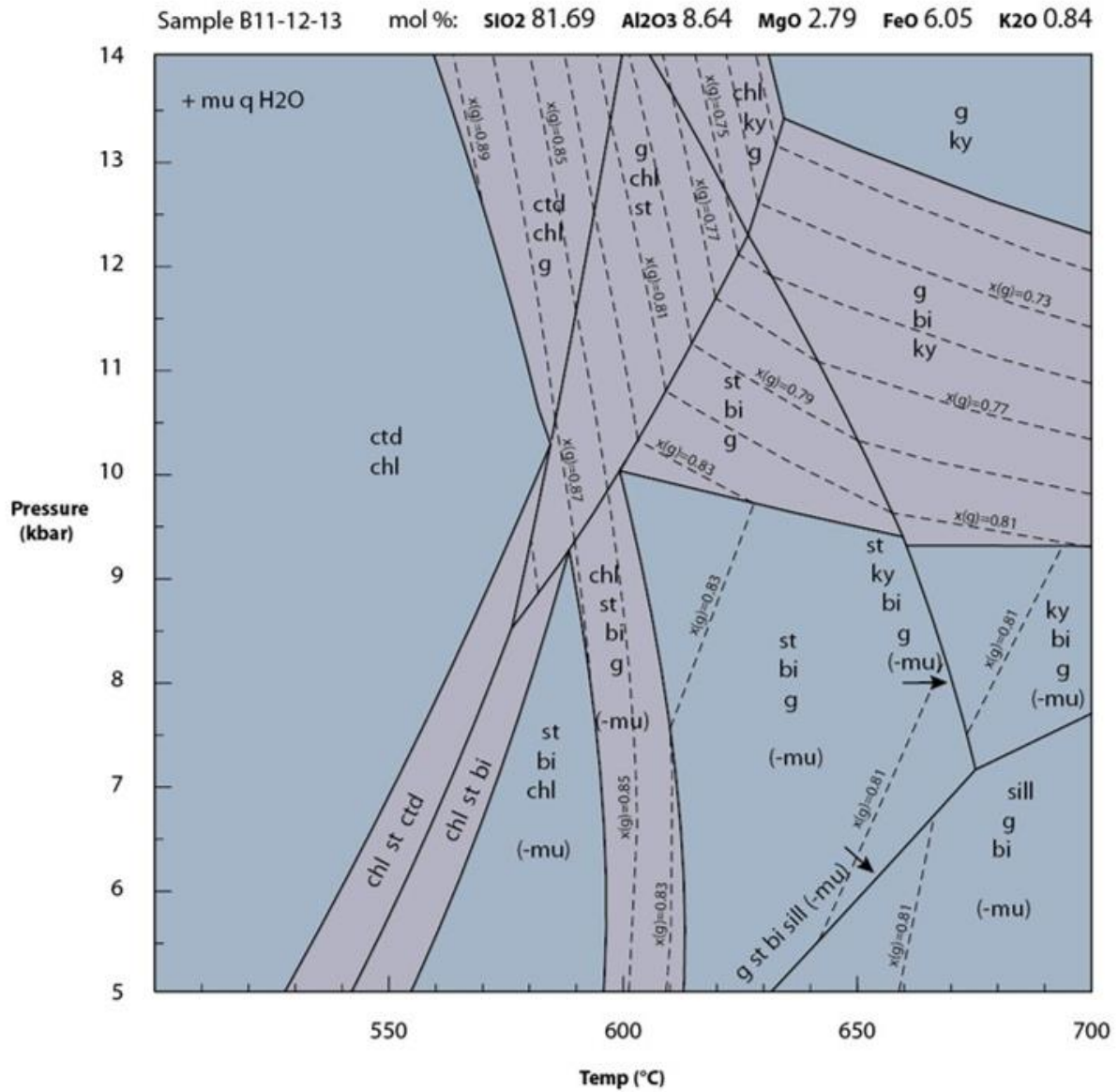
Minerals	Abbreviation	Chemical formulas (simplified)
quartz	q	SiO ₂
biotite	bi	K(Mg,Fe) ₃ (AlSi ₃ O ₁₀)(OH) ₂
muscovite	mu	KAl ₂ Si ₃ AlO ₁₀ (F,OH,Cl) ₂
chlorite	chl	(Mg,Fe,Al) ₃ (Si,Al) ₄ O ₁₀ (OH) ₂
garnet	g	(Mg,Fe,Mn) ₃ Al ₂ Si ₃ O ₁₂ (pyrope, almandine, spessartine)
garnet	g	Ca ₃ (Fe,Al,Cr) ₂ Si ₃ O ₁₂ (grossular, andraite, uvarovite)
water	H ₂ O	H ₂ O
chloritoid	ctd	(Fe,Mg,Mn) ₂ (Al,Fe)Al ₃ O ₂ (SiO ₄) ₄ (OH) ₄
staurolite	st	Fe ₂ Al ₉ O ₆ SiO ₄ (O,OH) ₂
kyanite	ky	Al ₂ SiO ₅
sillimanite	sill	Al ₂ SiO ₅
andalusite	and	Al ₂ SiO ₅
plagioclase	plag	CaAl ₂ Si ₂ O ₈ (anorthite) NaAlSi ₃ O ₈ (albite) (end members)

Pseudosections

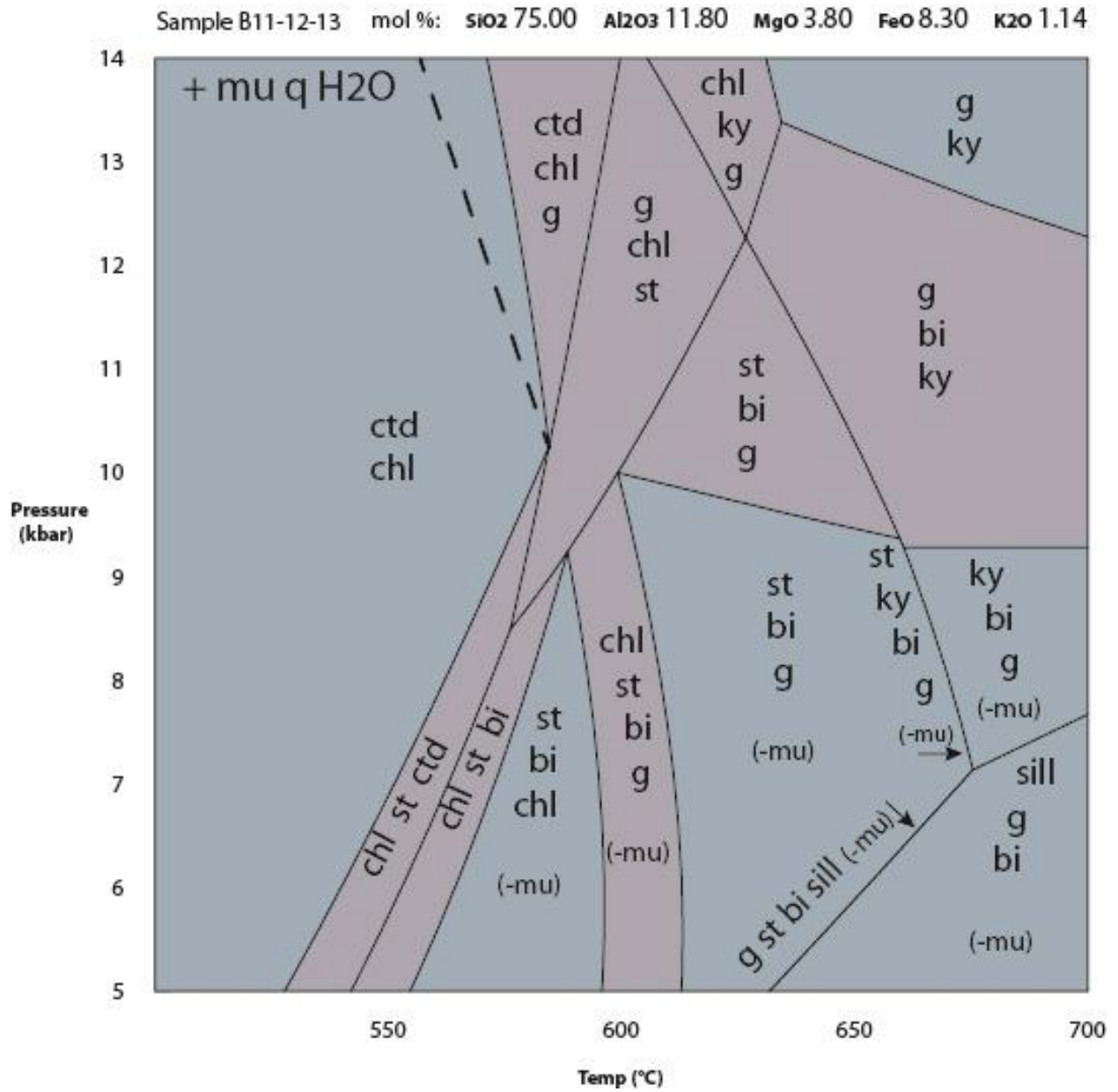
Pseudosection 1



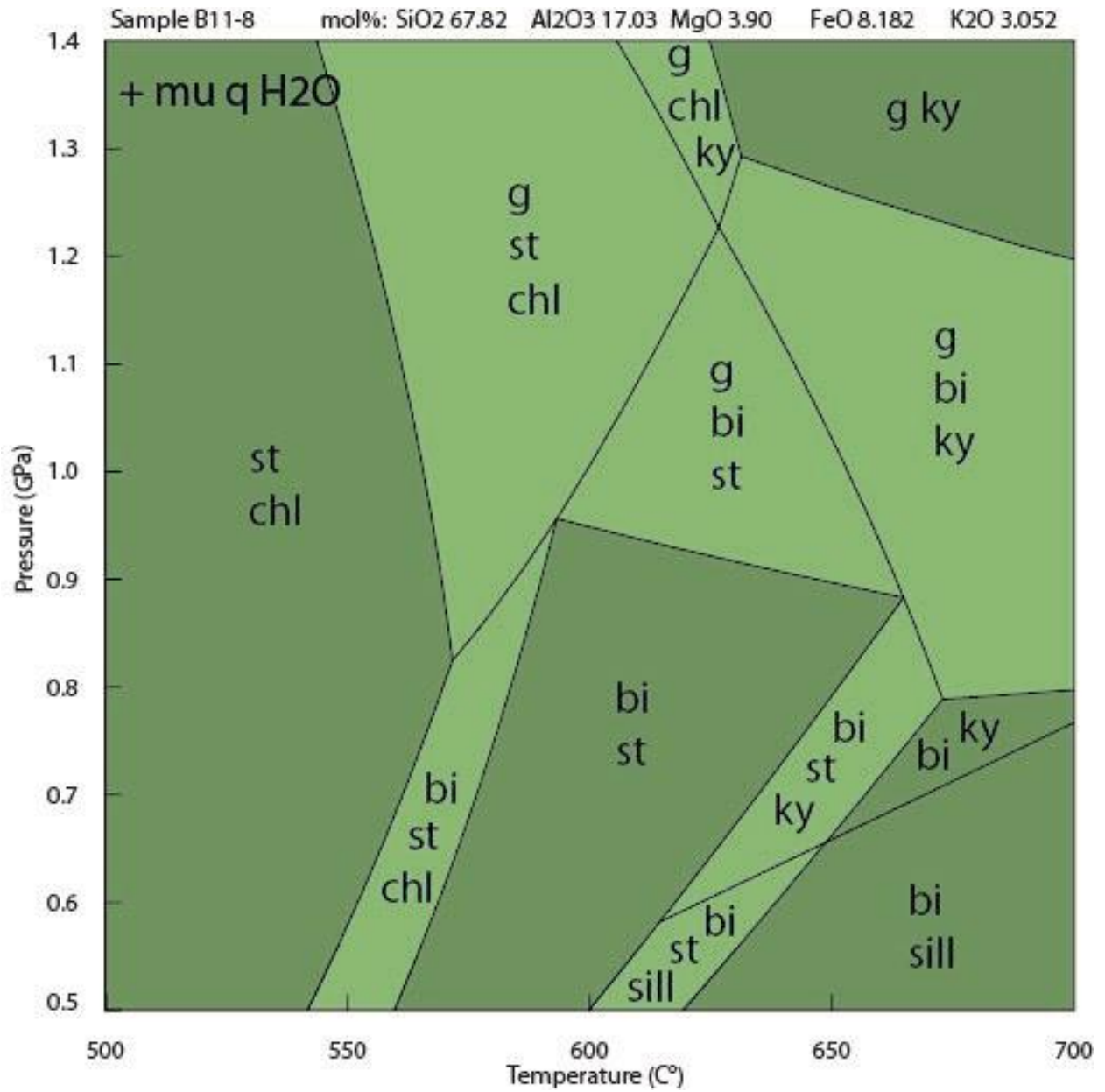
Pseudosection 3, same as pseudosection 1 but with garnet isopleths



Pseudosection 2. Lower SiO₂ amount than pseudosection 1



Pseudosection 4. Calculated by Josefin Linde (2013)



Pseudosection 5.

